THE JOURNAL OF BIOLOGICAL CHEMISTRY VOL. 290, NO. 2, pp. 727–743, January 9, 2015

Late Onset Neuropathy with Spontaneous Clinical Remission in Mice Lacking the POZ Domain of the Transcription Factor Myc-interacting Zinc Finger Protein 1 (Miz1) in Schwann Cells*

Received for publication, August 21, 2014, and in revised form, November 19, 2014 Published, JBC Papers in Press, November 21, 2014, DOI 10.1074/jbc.M114.605931

Adrián Sanz-Moreno[‡1], David Fuhrmann[‡1], Armin Zankel[§], Herbert Reingruber[§], Lara Kern[‡], Dies Meijer[¶], Axel Niemann[‖2], and Hans-Peter Elsässer[‡2,3]

From the [‡]Department of Cytobiology and Cytopathobiology, Philipps University of Marburg, Robert-Koch-Strasse 6, 35033 Marburg, Germany, [§]Graz University of Technology, 8010 Graz, Austria, [¶]Erasmus Medical Center, 3015GE Rotterdam, Netherlands, and [‖]ETH Zurich, CH-8093 Zurich, Switzerland

Background: The Myc-binding transcription factor Miz1 has multiple functions in different cells and tissues.
Results: Ablation of the Miz1 POZ domain in Schwann cells causes a late onset peripheral neuropathy with spontaneous remission.
Conclusion: Miz1 plays an essential role in myelin homeostasis of peripheral nerves.
Significance: Ablation of Miz1 function in Schwann cells leads to a new model for remitting peripheral neuropathies.

The transcription factor Miz1 (Myc-interacting zinc finger 1) is a known regulator of the cell cycle but also has cell cycle-independent functions. Here we analyzed the role of Miz1 in the peripheral nervous system, using an early embryonic conditional knock-out model in which the Miz1 POZ domain is ablated in Schwann cells. Although the development of myelinated nerve fibers was not impaired, *Miz1ΔPOZ* mice acquired behavioral signs of a peripheral neuropathy at the age of 3 months. At this time, ultrastructural analysis of the sciatic nerve showed de- and dysmyelination of fibers, with massive outfoldings and a focal infiltration of macrophages. Although the expression of genes encoding structural myelin proteins, such as periaxin, myelin basic protein, and myelin protein zero, was decreased, genes associated with a negative regulation of myelination, including c-*Jun*, *Sox2*, and *Id2*, were up-regulated in *Miz1ΔPOZ* mice compared with controls. In animals older than 4 months, the motor disabilities vanished, and the ultrastructure of the sciatic nerve exhibited numerous tomacula and remyelinated fibers, as indicated by thinner myelin. No second acute attack was observed up to the age of 1 year. Thus, the deletion of the Miz1 POZ domain in Schwann cells induces an acute neuropathy with a subsequent regeneration in which there is ongoing balancing between de- and remyelination. *Miz1ΔPOZ* mice are impaired in the maintenance of myelinated fibers and are a promising model for studying remyelination in adult peripheral nerves.

The transcription factor Miz1 (Myc-interacting zinc finger protein 1; Zbtb17) contains 13 zinc finger motifs in the middle and C-terminal parts of the protein and a BTB/POZ domain at the N terminus (1). DNA binding of a Miz1 tetramer (2, 3) occurs at the initiation region of target genes, and tetramerization depends on the POZ domain (4, 5). Miz1 can either activate or repress transcription, depending on its binding partners. Coactivators include nucleophosmin and p300, and known corepressors are Myc, Bcl-6, Gfi1, and Zbtb4 (6). Miz1 has a broad expression profile and has also been detected in neural precursor cells (7, 8) and in different parts of the adult brain (9, 10). The constitutive knockout of *Miz1* is lethal on embryonic day 7.5 (7). Miz1 function in skin, the hematopoietic system, mammary gland, and neurons of the central nervous system has been investigated in a conditional knock-out mouse model by deletion of the POZ domain encoded by exons 3 and 4 of the *Miz1* gene (also known as *Zbtb17*) (2, 3, 10–13).

In the peripheral nervous system, Schwann cells are the myelin-forming cells and remain tightly connected to the axon (14–16). This connection is lost following a nerve injury because the axon degenerates distally from the lesion. Schwann cells engaging this degenerating segment dedifferentiate and finally remyelinate the regrowing fiber. Molecular pathways driving these de- and redifferentiation processes have been elucidated (17, 18). Thereby, $p21^{Cip1}$, encoded by the Miz1 target gene *Cdkn1a*, is central in the regulation of Schwann cell proliferation following a nerve injury as well as in development (19). An important signaling pathway driving demyelination and dedifferentiation of Schwann cells is the Ras/Raf/MEK/ERK pathway (20), which is accompanied by an inflammatory response to support the removal of tissue debris (21). Interestingly, activated Ras can also cause oncogene-induced senescence (22) by activating $p53/p21^{Cip1}$ and $p16^{INK4a}$ (23).

Here we ask whether a Schwann cell-specific POZ domain deletion of *Miz1* has an impact on peripheral nerve myelination. We show that *Miz1ΔPOZ* mice develop a late onset peripheral neuropathy characterized by de- and dysmyelination, increased levels of $p21^{Cip1}$, and elevated senescence mark-

* This work was supported by Deutsche Forschungsgemeinschaft Grant EL-125/6-1.
[1] Both authors contributed equally to this work.
[2] Both authors contributed equally to this work.
[3] To whom correspondence should be addressed. Tel.: 49-64212864075; Fax: 49-64212864075; E-mail: elsaesse@mailer.uni-marburg.de.

ers. Finally, the neuropathy progresses to a spontaneous clinical remission.

EXPERIMENTAL PROCEDURES

Mice—Miz1$^{lox/lox}$ mice (2, 11) were crossed with the desert hedgehog (*Dhh*)-*Cre* driver line (C57Bl6-Tg(Dhh-cre)1Mejr) (24) to achieve conditional ablation in Schwann cells of *Miz1* exons 3 and 4, which encode the POZ domain. Mice had a mixed C57Bl6 and 129S2/SvHsd genetic background. Here, animals that were *Dhh-Cre*$^{+}$;*Miz1*$^{flox/flox}$ are designated *Miz*Δ*POZ*, whereas *Dhh-Cre*$^{-}$;*Miz1*$^{flox/flox}$ mice were used as control animals and named *Ctr*. Genotyping was performed by standard PCR, using the REDExtract-N-Amp tissue PCR kit (XNATR; Sigma). Primers used for genotyping are listed in Table 1.

Research with mice was conducted according to the German Animal Protection Law (Tierschutzgesetz). The application for the experiments was reviewed and approved by the responsible local authorities (Regierungspraesidium Giessen, reference numbers V54-19c20 15-MR20/10 Nr. A18/2010 and V54-19c20 15h01-MR20/10 Nr. 14/2014).

Clinical Assessment—To assess the degree of motility impairment, the score devised by King *et al.* (25) was used. Mice were judged in five categories: leg cross, grid walk, hind and front leg grasp, and tail bending. Scores from 0 = normal to 2 = abnormal were given in each category, resulting in overall scores between 0 and 10 (normal to highly impaired). Scoring was performed independently by two observers blinded to the animals' age and genotype. Walking pattern (26) was documented for control and *Miz1*Δ*POZ* mice by dipping foot pads of the hind paws into India ink and allowing the animal to walk on 50 × 10-cm paper strips placed in a dark runway of 10-cm height. Mice were habituated to the runway for 5 min, and then four runs were performed. To measure the grip strength of the forelimbs (27), mice were picked up by the tail and allowed to grasp a metal bar (1.5-mm diameter) attached to a spring balance. Then animals were gently pulled back, and the force at which they released the bar was determined. Each mouse was tested three times in a row with 30-s breaks between each trial.

Immunohistology—Sciatic nerve fragments were fixed overnight at 4 °C either in phosphate-buffered 3.5% formaldehyde (staining for Miz1, Sox10, Ki67, neurofilament-M, and unphosphorylated neurofilament-H/SMI32) or in a mixture of 60% ethanol, 30% chloroform, and 10% acetic acid (staining for p21^{Cip1}, F4/80, c-Jun, S100, and histone 3 trimethylated on lysine 9 (H3K9me3)).[4] After fixation, tissue was dehydrated and embedded in paraffin according to standard procedures. For antigen retrieval, sections were treated for 20 min in a steam cooker (Braun, Germany) in 10 mM Tris buffer (pH 9) containing 1 mM EDTA (staining for Miz1, neurofilament-M, Ki67, unphosphorylated neurofilament-H/SMI32, and Sox10); for 20 min (staining for p21^{Cip1}, H3K9me3, c-Jun, and S100) in a steam cooker in 10 mM citrate buffer (pH 6); or for 6 min with proteinase K (20 μg/ml) in phosphate-buffered saline at room temperature (staining for F4/80). Antibody staining was performed according to standard procedures using appropriate biotinylated secondary antibodies, streptavidin labeled with peroxidase (KPL), and 3-amino-9-ethylcarbazole for visualization. Alternatively, secondary antibodies labeled with Alexa 488 or Alexa 546 (Invitrogen) were used for immunofluorescence microscopy. The following primary antibodies were used: Miz1 (1:100; 10E2) (28), p21^{Cip1} (1:100; Abcam, ab2961), F4/80 (1:50; Serotec, MCA497GA), H3K9me3 (1:1000; Abcam, ab8898), c-Jun (1:25; Cell Signaling, catalog no. 9165), S100B (1:150; Novus Biologicals, NBP1-22763), neurofilament-M (1:200; Millipore, AB1987), unphosphorylated neurofilament-H (1:200; Covance, SMI-32R), Sox10 (prediluted; DCS, S1058R06), and Ki67 (1:500; Abcam, ab15580). Stained sections were mounted in Mowiol 4-88 (Roth GmbH, Karlsruhe, Germany) according to the manufacturer's recommendations.

Senescence-associated (SA) β-Galactosidase Staining—Sciatic nerve pieces were fixed for 1 h at 4 °C in 4% phosphate-buffered paraformaldehyde (2 ml/sample) with gentle rotation. Subsequently, the tissue was washed three times for 20 min in LacZ rinse buffer (40 mM citrate buffer, pH 6, 2 mM $MgCl_2$, 0.02% Nonidet P-40, 0.01% sodium desoxycholate, and 150 mM NaCl) at room temperature. Then tissue was incubated in LacZ rinse buffer containing 5 mM potassium hexacyanidoferrate (III), 5 mM potassium hexacyanidoferrate (II), and 1 mg/ml X-Gal (Roth) at 37 °C overnight.

Succinate Dehydrogenase Staining—Calf muscles were prepared, covered with Tissue-Tek O.C.T. Compound (Sakura, Netherlands) and quick frozen in isopentane cooled by liquid nitrogen. Cryostat sections were air-dried and subsequently incubated in a 37 °C prewarmed solution containing 0.1 M phosphate buffer, pH 7.6, 0.1 M sodium succinate, and 0.1% nitro blue tetrazolium chloride (Applichem, Darmstadt, Germany) for 1 h. Slides were rinsed in water, dehydrated with ethanol, incubated in xylene, and embedded in Entelan (Merck Millipore).

Ultrastructural Analysis—Sciatic nerve fragments were fixed in a mixture of 2.5% glutaraldehyde, 2.5% paraformaldehyde, and 0.05% picric acid in 67 mM cacodylate buffer (pH 7.4) according to Ito and Karnovsky (29). Postfixation was performed in 1% osmium tetroxide followed by an overnight incubation with 0.3% uranyl acetate dissolved in 50 mM maleate buffer (pH 5). Samples were embedded in Epon according to standard procedures. Thin sections were contrasted with lead citrate and examined with a Zeiss EM 109S electron microscope.

Three-dimensional Reconstructions—For the generation of three-dimensional reconstructions, serial block-faced scanning electron microscopy (30) was performed using a prototype *in situ* ultramicrotome from Gatan (Pleasanton, CA) and an environmental scanning electron microscope (FEI ESEM Quanta 600 FEG, FEI, Eindhoven, Netherlands). For imaging, backscattered electrons were used, resulting from primary electrons with an energy of 4 keV. Serial sectioning and imaging was done in the low vacuum mode of the environmental scanning electron microscope with water vapor as imaging gas at a pressure of about 107 pascals. The chemically pretreated sample blocks were trimmed to small cuboids of about 300 × 400 × 500 μm^3 using a Diatome® diamond knife "Trim 90" and then glued on

[4] The abbreviations used are: H3K9me3, histone 3 trimethylated on lysine 9; SA, senescence-associated; P*n*, postnatal day *n*; P0, myelin protein zero.

TABLE 1
List of PCR primers

QUANTITATIVE PCR PRIMERS			
Ambra1	**fw:** GAGCACCCAATTTACCCAGA **rv:** GATCATCCTCTGGGCGTAGTA	***Mtmr2***	**fw:** GGAAACTGTATGACCCCCTTC **rv:** CACAGAGTTCATAGCGTTCATTTATC
Ccl2	**fw:** CATCCACGTGTTGGCTCA **rv:** GATCATCTTGCTGGTGAATGAGT	***Mtmr6***	**fw:** GCCAAATACAGCCTCTTTCAA **rv:** AATTATGCTCAGCACAGACTGC
Ccl3	**fw:** TGCCCTTGCTGTTCTTCTCT **rv:** GTGGAATCTTCCGGCTGTAG	***Mtmr7***	**fw:** ACCTCATGGCTGTGAAGGA **rv:** CATGTAAGTGGACTTTCTGAATTTTT
Ccnd1	**fw:** TTTCTTTCCAGAGTCATCAAGTGT **rv:** TGACTCCAGAAGGGCTTCAA	***Mtmr9***	**fw:** GCAGGACAACACGGAGGA **rv:** ACCCAGAGAGCCCACAAAT
Cxcl10	**fw:** GCTGCCGTCATTTTCTGC **rv:** TCTCACTGGCCCGTCATC	***Mtmr11***	**fw:** GTAACCTTCCAGCCTTGTGG **rv:** CTTGACAAGCCGCTCACAG
Cxcl14	**fw:** GACCAGACGGCAGGAGCAC **rv:** TTTCAAGCACGCCTCTCTC	***Mtmr13***	**fw:** CAACAGCATCGTCACAAACA **rv:** CCGAATCTTCAAACCCACTC
Dctn6	**fw:** CTCCCGGAGCAGTAGTGTGT **rv:** AGGGTGGATCACCGTCCT	***Ngfr***	**fw:** ACTGAGCGCCAGTTACGC **rv:** CGTAGACCTTGTGATCCATCG
Dlg1	**fw:** TTTCCCGAAAATTTCCCTTC **rv:** TGGCATTAGAAGTTACGTGCTG	***Nrg1 (I)***	**fw:** GGGAAGGGCAAGAAGAAGG **rv:** TTTCACACCGAAGCACGAGC
Egr1	**fw:** CCTATGAGCACCTGACCACA **rv:** TCGTTTGGCTGGGATAACTC	***Pikfyve***	**fw:** GGCCGACTGATCTGGATTC **rv:** CCAGCAAATGACCATCAAATAC
Exoc2	**fw:** GGGAGAACCTGGGTACTGGT **rv:** CCGTGAGGAGGCAATTATGT	***Pten***	**fw:** AGGCACAAGAGGCCCTAGAT **rv:** CTGACTGGGAATTGTGACTCC
Exoc4	**fw:** TGACCAACATCACCATGTCA **rv:** GCTGTGTTGTACAGCATCTCG	***Prx***	**fw:** AGGAGCTCTGGAGGTGTCTGG **rv:** TCTTGAGTGATGGCCTTTTC
Emr1	**Fw:** GGAGGACTTCTCCAAGCC **Rv:** AGGCCTCTCAGACTTCTG	***Rorc***	**fw:** ACCTCTTTTCACGGGAGGA **rv:** TCCCACATCTCCCACATTG
Fgd4	**fw:** TACATGTATGGCGCTCCTCA **rv:** CTTAGGCATATCATCCACAACG	***Rufy***	**fw:** TGATGCAAAAGAAGCTTTCTGA **rv:** TGAGGGCATTGACTTCATAGA
Gapdh	**fw:** CATGGCCTTCCGTGTTCCTA **rv:** GCGGCACGTCAGATCCA	***Saa1***	**fw:** CCAGGATGAAGCTCACCA **rv:** TAGGCTCGCCACATGTCC
Id2	**fw:** GACAGAACCAGGCGTCCA **rv:** AGCTCAGAAGGGAATTCAGATG	***Saa2***	**fw:** TTCATTTATTGGGGAGGCTTT **rv:** GCCAGCTTCCTTCATGTCAG
c-Jun	**fw:** CCAGAAGATGGTGTGGTGTTT **rv:** CTGACCCTCTCCCCTTGC	***Sh3tc2***	**fw:** GGCCGACTCACTTTCTACCA **rv:** GCTAGCGCCAGCAGAAAAT
Lrp12	**fw:** CAGGCTGGCGTATTTTTCA **rv:** ATTTCCACAGCGGAACTGAT	***Sox2***	**fw:** TCCAAAAACTAATCACAACAATCG **rv:** GAAGTGCAATTGGGATGAAAA
Mbp	**fw:** TGGCCACAGCAAGTACCAT **rv:** AGTCAAGGATGCCCGTGT	***Spast***	**fw:** CAGCCCTGGGTCCTATCC **rv:** TTCTCATCTCACTGGCAGACAT
Miz1	**fw:** AGGCACACTGTCTGAGAAGAGA **rv:** TGGTTCAGCTGCTCCAAGA	***Vamp4***	**fw:** TGCAAGAGAATATTACAAAGGTAATTG **rv:** GAAAGCGGTGGCATTATCC
Mpz	**fw:** CCCTGGCCATTGTGGTTTAC **rv:** CCATTCACTGGACCAGAAGGAG	***Vps13d***	**fw:** CTGACTAACCTAGAGCACCAGATCTAT **rv:** TGTGGTTCCGAAGAGCAAA
Mtmr1	**fw:** AAAGTGGCAGCCTTTCGAG **rv:** TGGCTGCAACGTGTAATTGT	***Vps28***	**fw:** AGCTTCTGTCGCCATCTCC **rv:** CCCAGGCAGCTATACAGCAC
GENOTYPING PRIMERS			
Cre	**fw:** GAACGCACTGATTTCGACCA **rv:** AACCAGCGTTTTCGTTCTGC		
Miz1	**Primer 1:** GTATTCTGCTGTGGGGCTATC **Primer 2:** GGCTGTGCTGGGGGAAATC **Primer 3:** GGCAGTTACAGGCTCAGGTG		

special aluminum rivets with superglue (31). A voxel size of 74 × 74 × 100 nm^3 is determined by a slice thickness of 100 nm and a pixel resolution of 1024 × 1024 at an image width of 76 μm. Three-dimensional models were created with the Avizo® Fire software (Visualization Sciences Group, Mérignac, France).

Morphometric Analysis—Morphometric analyses of the sciatic nerve were performed blinded on electron microscopic images taken at ×1100 magnification. The g-ratios of 100–120 randomly selected myelinated fibers were determined in each of three or four animals per genotype and time point. Morphological alterations (myelin outfoldings and aberrant axonal features) were determined for all myelinated axons on 10–17 randomly chosen EM pictures per animal. Between three and eight animals were analyzed per genotype and time point, resulting in the blinded counting of 1200–5000 fibers/data point.

Nerve sections were double-stained for neurofilament-M (secondary antibody labeled with Alexa-488) and unphosphorylated neurofilament-H (secondary antibody labeled with Alexa-546), and three randomly chosen pictures were taken from each individual sample with a fixed exposure time for each fluorochrome (10 ms for Alexa-488; 100 ms for Alexa-546). Intensities were evaluated with Adobe Photoshop, and the ratio of the fluorescence intensities was calculated. Nerve tissue from four individual animals was analyzed for each genotype.

RNA Isolation and Quantitative PCR—Sciatic nerve pieces were stored in RNAlater (Sigma, R0901) until homogenization in TRI Reagent (Sigma, T9424). RNA was extracted, DNase-treated (Macherey-Nagel, catalog no. 740963), and further purified using a NucleoSpin RNA column-based kit (Macherey-Nagel, catalog no. 740948) according to the manufacturer's instructions. 0.1 μg of total RNA was reverse transcribed with the RevertAid first strand cDNA synthesis kit (Thermo Scientific, catalog no. K1622) using random hexamer primers. SYBR Green-based real-time polymerase chain reactions (Thermo Scientific, AB1167) were run in triplicate using a Mx3005P quantitative PCR system (Stratagene, Heidelberg, Germany) and undiluted cDNA. Gene expression was normalized to GAPDH and analyzed by the comparative cycle threshold method ($\Delta\Delta Ct$). "No template controls" were included in each run, and product specificity was verified by dissociation curve analysis. The primers used are summarized in Table 1.

Statistics—Comparisons between *Ctr* and *Miz1*Δ*POZ* animals were analyzed by two-tailed Student's *t* tests. All statistical tests were performed with Prism version 5.0 software (GraphPad) (not significant, $p > 0.05$; *, $p = 0.01–0.05$; **, $p = 0.001–0.01$; ***, $p < 0.001$. Data are shown as mean ± S.D.

RESULTS

Deletion of the Miz1 POZ Domain in Schwann Cells—Because Miz1 expression in the peripheral nervous system had not been elucidated in detail, we analyzed it in the sciatic nerve at different time points after birth by immunohistochemistry. Miz1 expression was detected in sciatic nerve samples on days 10, 30, 60, and 90 postpartum (Fig. 1*A*), and the Miz1 signal colocalized to the SOX-10-positive Schwann cell nuclei (Fig. 1*B* representative for all time points). Consistently, expression of Miz1 mRNA levels was similar at these four postnatal time points in sciatic nerve lysates, as determined by quantitative RT-PCR (Fig. 1*C*).

To study the functional relevance of Miz1 expression in Schwann cells, we used a mouse model in which *Miz1* exons 3 and 4 are flanked by *loxP* sites, leading to a truncated form of Miz1 lacking the POZ domain upon Cre-mediated recombination (2, 11) (Fig. 1*D*). We crossed $Miz1^{lox/lox}$ mice with a transgenic mouse line expressing the Cre recombinase under the control of desert hedgehog gene (*Dhh*) regulatory elements (32). This construct drives Cre expression in the Schwann cell lineage from embryonic day 12 onward (33). $Miz1^{lox/lox}$ animals either expressing Cre (*Miz1*Δ*POZ*) or not expressing it (*Ctr*; control) were employed. Deletion of exons 3 and 4 was evaluated by PCR using DNA isolated from skin and from sciatic nerve samples (Fig. 1*D*).

The embryonic deletion of the Miz1 POZ domain driven by the *Dhh-Cre* is not embryonic lethal, unlike in the case of the constitutive knockout of Miz1 (7), and mutant mice were born in normal Mendelian ratios (data not shown). We could not identify major differences between 30-day-old *Ctr* and *Miz1*Δ*POZ* nerves on semithin sections (data not shown) or in electron microscopic pictures (Fig. 1*E*). The arrangement and density of nerve fibers, the g-ratio (Fig. 1*F*), and the axon and nerve diameters were similar in 30-day-old *Ctr* and *Miz1*Δ*POZ* mice, indicating that the deletion of the Miz1 POZ domain has no major impact on peripheral nerve development within the first 30 postnatal days.

Phenotype of Postnatal Day 90 (P90) to P120 Mice—*Miz1*Δ*POZ* mice did not show an obvious behavioral phenotype during the first 2 months after birth. In contrast, P90 *Miz1*Δ*POZ* animals displayed characteristic signs of a peripheral neuropathy, with cramping of hind limbs and gait abnormalities on plain and smooth surfaces (data not shown). When placed on a grid, *Miz1*Δ*POZ* mice were hardly able to walk over the grid because they could not grab the bars properly, and their hind legs dropped between them (Fig. 2*A*). Thus, 3-month-old mice with a Miz1 POZ domain deletion in Schwann cells exhibited notable motor disorders.

In order to document the motor disorder in more detail, we analyzed animals of different ages using a score sheet as originally described by King *et al.* (25) and further used by others (34, 35). The mean score value was not different between P60 control and *Miz1*Δ*POZ* animals. However, P90 and P120 *Miz1*Δ*POZ* mice exhibited a significant increase of the mean score value (Fig. 2*B*). This was confirmed also in a footprint assay by brush marks of the hind limbs seen in P90 and P120 *Miz1*Δ*POZ* but not in control animals, whereas P60 *Miz1*Δ*POZ* animals showed normal footprints (Fig. 2*C*). Finally, a grip assay was performed to test the strength of the forelimbs, which was lower in P120 male (Fig. 2*D*) and female (data not shown) *Miz1*Δ*POZ* mice, compared with control mice.

To characterize the underlying neuropathy, sciatic nerve samples were analyzed by light and transmission electron microscopy. Semithin sections of the sciatic nerves from P90 *Miz1*Δ*POZ* mice showed fewer myelinated fibers per field of view, with corresponding larger areas of endoneurial space (Fig. 3*A*). In addition, myelin outfoldings and signs of demyelination were present in semithin sections of *Miz1*Δ*POZ* animals, which

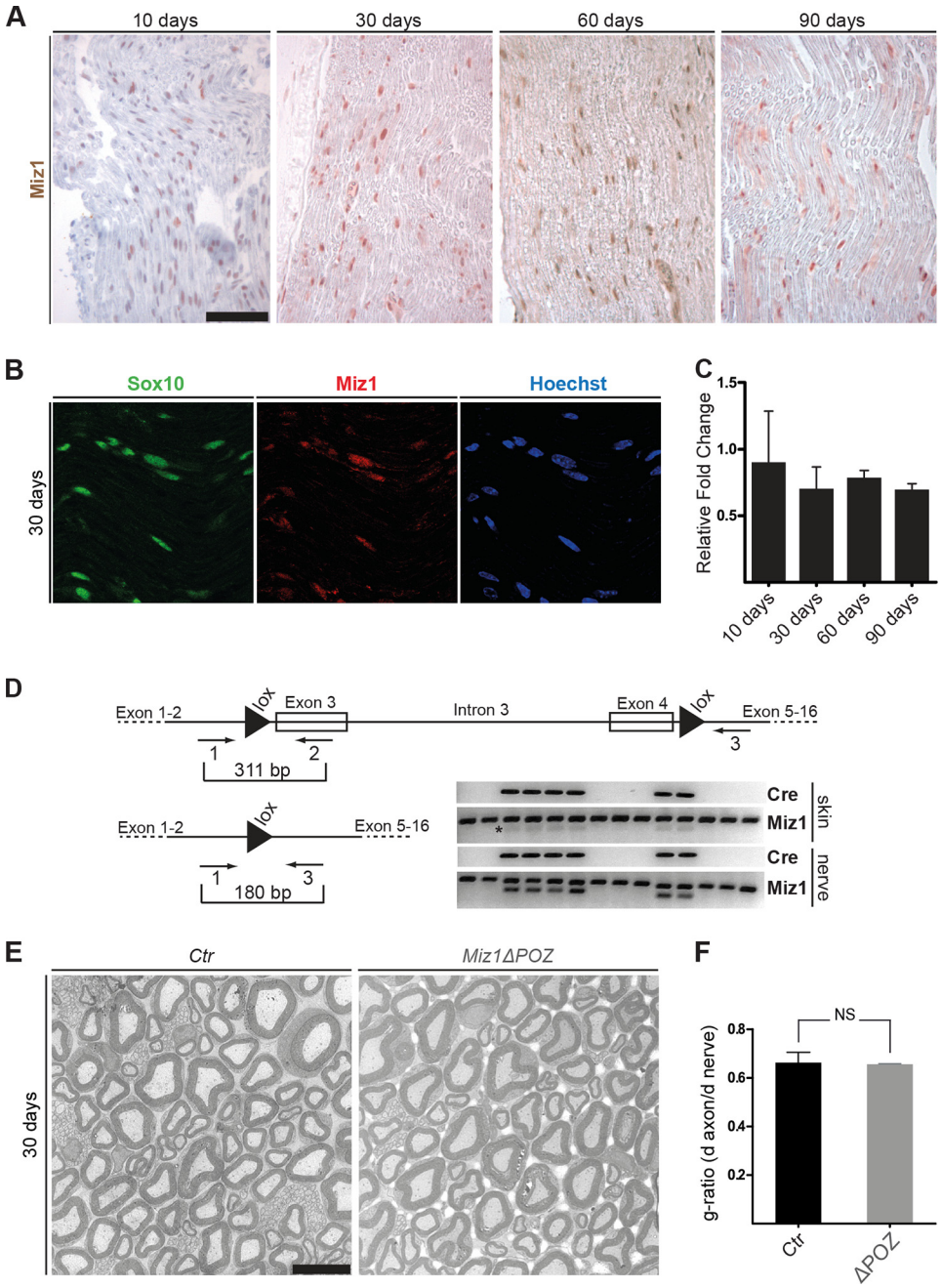

FIGURE 1. **Expression of Miz1 in peripheral nerves and conditional knockout of the Miz1 POZ domain in Schwann cells.** *A*, immunohistochemical stainings of Miz1 in sciatic nerve tissue from control mice of different ages, as indicated. *B*, confocal double immunofluorescence pictures from stainings of nerve tissue from P30 control mice using antibodies against Miz1 and Sox10. *C*, expression of Miz1 mRNA measured by quantitative RT-PCR. $n = 3$ independent samples were used for each time point, whereas each sample contained sciatic nerve tissue from three mice at P10, from two mice at P30, and from one mouse at P90, respectively. *D*, exons 3 and 4 encoding the Miz1 POZ domain were flanked with *loxP* sites. The indicated primers (*arrows*) were chosen to discriminate between the floxed allele (311 bp) and the recombined allele (180 bp), respectively (see Table 1 for primer sequences). The gel shows a representative PCR analysis with genomic DNA isolated either from skin or from sciatic nerve and performed with primers for Cre recombinase and Miz1. *, faint bands most likely arising from nerve tissue in the skin. *E*, low power electron microscopic pictures from sciatic nerves of P30 control and *Miz1ΔPOZ* mice. *F*, average g-ratios obtained from electron microscopic pictures, as shown in *E*. *Bar*, 50 μm (*A*), 10 μm (*B*), and 5 μm (*E*). NS, not significant. *Error bars*, S.D.

were confirmed by ultrastructural analysis (Fig. 3*B*). In blinded countings, using low power electron microscopic sections, a significant proportion of myelinated axons exhibited aberrant myelin structures and axonal impairment in *Miz1ΔPOZ* animals compared with controls (Fig. 3*C*). However, myelinated fibers without outfoldings had a normal g-ratio, independent of the axonal caliber (Fig. 3*D*).

To determine whether myelin fragments present on ultrathin cross-sections are completely separated from the myelin sheet or represent cuts through longitudinal outfoldings, we performed serial block-faced scanning electron microscopy for a three-dimensional reconstruction of P90 nerves. Myelin of control animals formed a tube-like structure around the enwrapped axon without major extensions toward the axon or

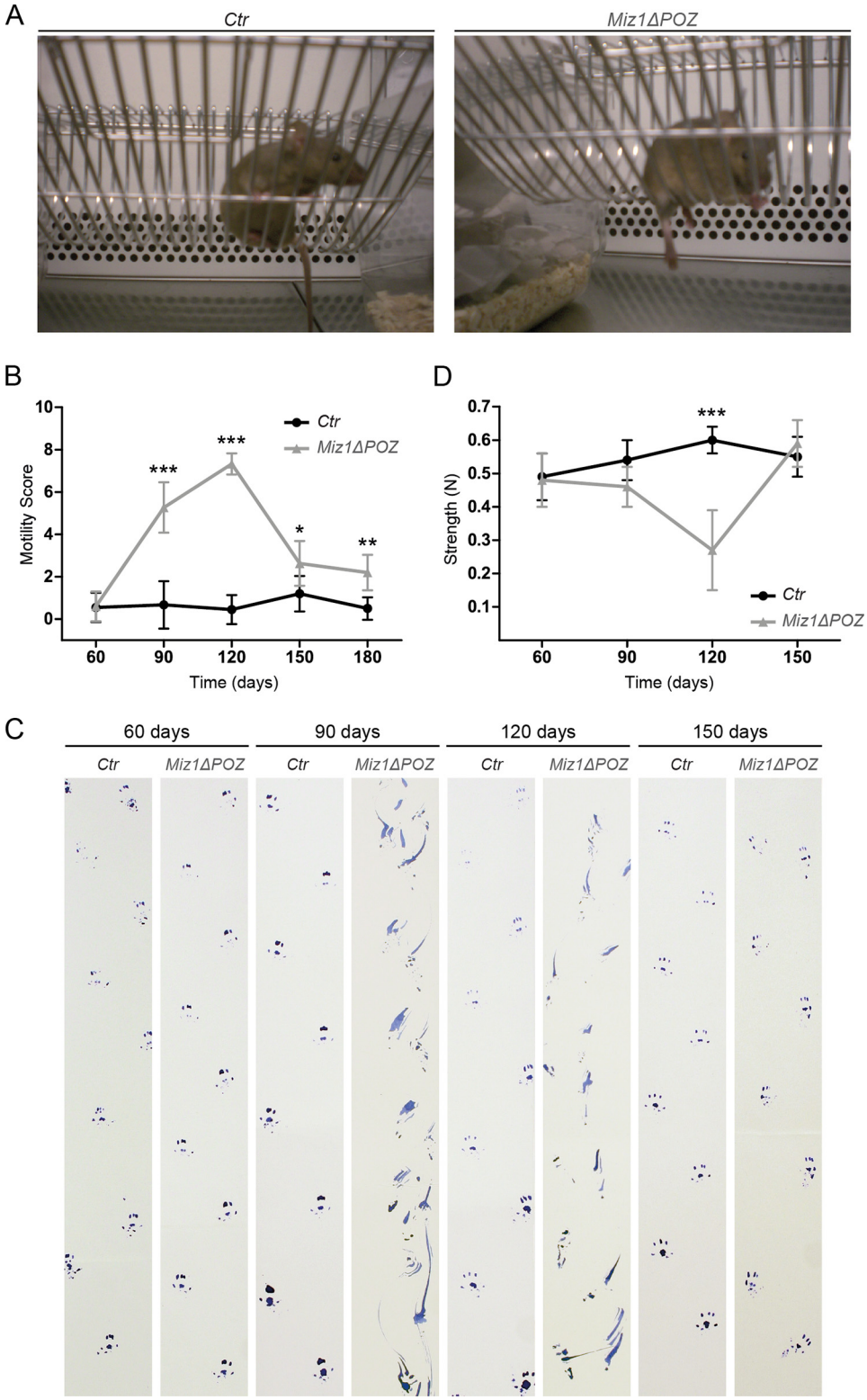

FIGURE 2. **Motor disabilities of P90 to P120 *Miz1ΔPOZ* animals.** *A*, whereas control mice moved properly on the cage bars (*left*), *Miz1ΔPOZ* animals could not grab the bars with their hind paws, and the hind limbs dropped between the cage bars (*right*). *B*, time course of the motility score obtained as described under "Experimental Procedures." *C*, footprint assay of P60, P90, P120, and P150 *Ctr* and *Miz1ΔPOZ* mice. Note the occurrence of brush marks in the case of *Miz1ΔPOZ* mice at P90 and P120, which disappeared completely until P150. *D*, grip strength of the forelimbs of P60, P90, P120, and P150 *Ctr* and *Miz1ΔPOZ* male mice. *Error bars*, S.D.

the cytoplasmic space (Fig. 4, *A* and *B*). In contrast, myelin sheets from *Miz1ΔPOZ* nerve fibers exhibited outfoldings and cytoplasmic myelin fragments in ultrastructural sections and possessed multiple excrescences with variable morphology yet still connected to the original myelin sheet (Fig. 4, *C* and *D*). Conversely, outfoldings and myelin fragments observed in thin

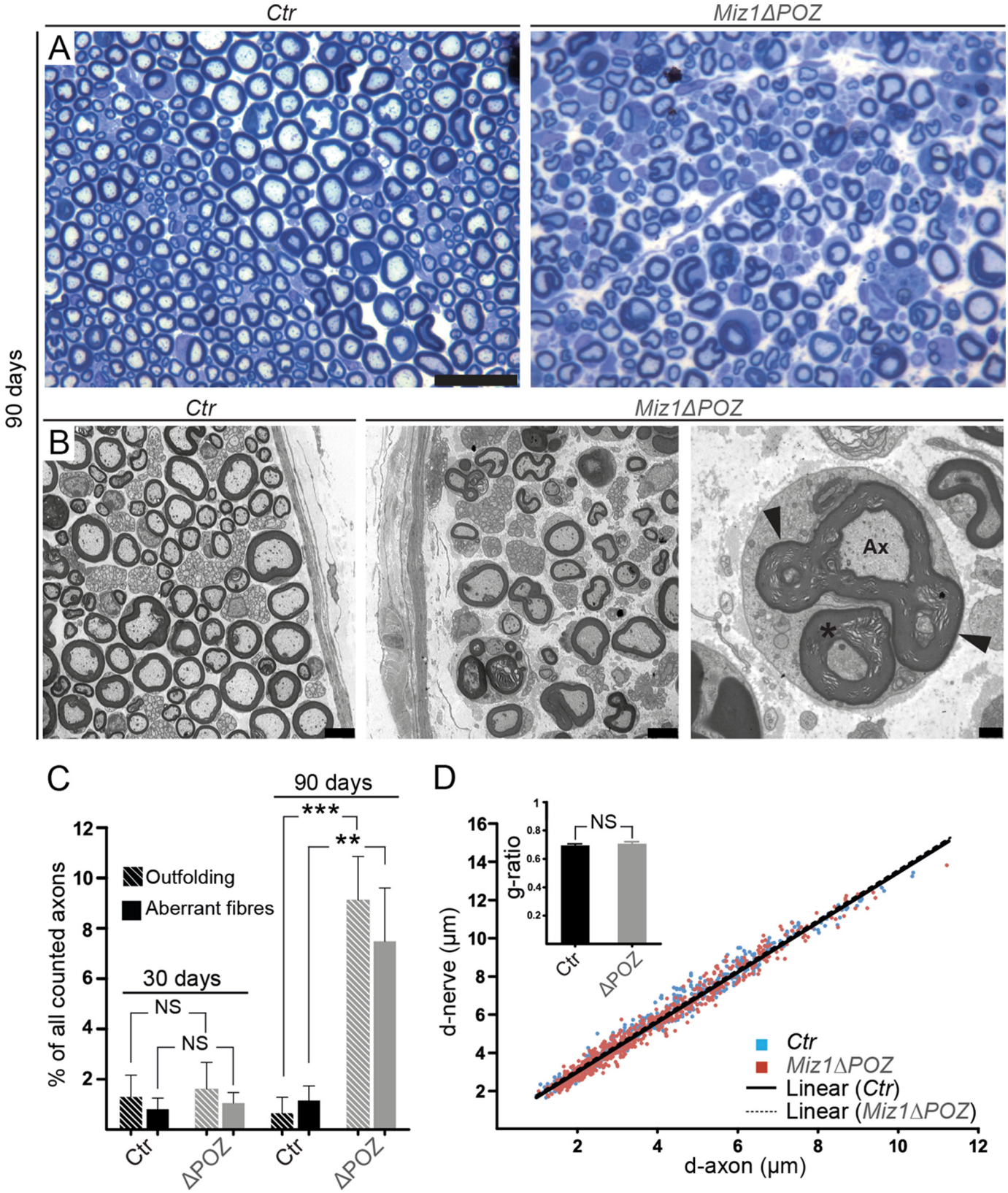

FIGURE 3. **Motor disabilities are accompanied by structural changes in the sciatic nerves of P90 *Miz1ΔPOZ* mice.** *A*, light microscopy of 1-μm thin sections from sciatic nerves of control (*left*) and *Miz1ΔPOZ* mice (*right*). *B*, low power electron microscope pictures (*left*) from control and *Miz1ΔPOZ* animals. The *right-hand image* shows a higher magnification of a Schwann cell with a myelinated axon (*Ax*) and outfoldings (*arrowheads* and *asterisk*). *C*, percentage of nerve fibers exhibiting outfoldings and other aberrantly myelinated fibers in sciatic nerves of control and *Miz1ΔPOZ* mice. *D*, scatter plot correlating the diameter of the axon with the diameter of the entire nerve fiber in sciatic nerves from P90 control and *Miz1ΔPOZ* mice. *Inset*, g-ratios of nerve fibers from the sciatic nerves of control and *Miz1ΔPOZ* mice. *Bar*, 25 μm (*A*), 23 μm (*B*, *left* and *middle*), and 900 nm (*B*, *right*). *Error bars*, S.D. **, $p = 0.001–0.01$; ***, $p < 0.001$; *NS*, not significant ($p > 0.05$).

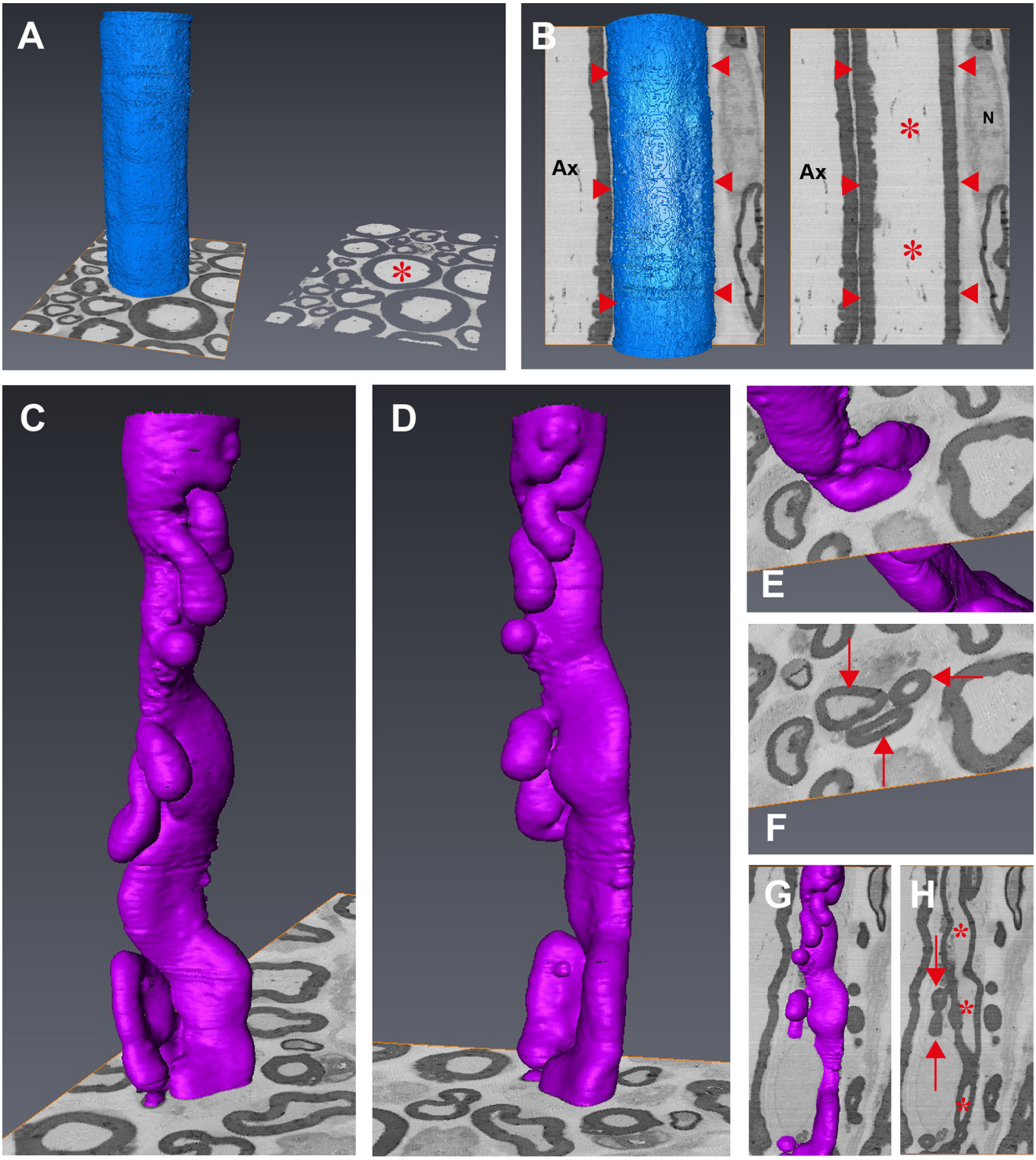

FIGURE 4. **Three-dimensional reconstruction of nerve fibers using serial block-faced scanning electron microscopy.** *A*, sciatic nerve fiber of a P90 control animal reconstructed from 300 consecutive 100-nm-thick sections. On the *right*, the *red asterisk* marks the cross-section that has been reconstructed on the *left*. *B*, same nerve fiber as in *A* aligned to a central longitudinal plane. *Arrowheads*, surface of the reconstructed myelin sheet; *asterisks*, corresponding axon. *Ax*, adjacent axon. *N*, nucleus. *C*, nerve fiber from the sciatic nerve of a P90 *Miz1ΔPOZ* mouse reconstructed from 400 consecutive 100-nm-thick sections. *D*, same as in *C* but rotated 45° around the longitudinal axis. *E* and *F*, these pictures show part of *C*, providing the reconstruction with one section (*E*) and the section alone (*F*). *Arrows* in *F*, intracellular myelin structures at the position shown in *E*. *G* and *H*, longitudinal alignment of the myelin sheet reconstruction analogous to that shown in *B*. *Arrows*, intracellular myelin structures; *asterisks*, axon enwrapped by the myelin sheet.

sections could be related to the myelin excrescences (Fig. 4, *E–H*). Thus, the nerve ultrastructure reflects a massive blebbing of the myelin sheaths.

Besides degenerative structures, signs of remyelination were detectable in P90 sciatic nerves of *Miz1ΔPOZ* mice. Larger caliber axons without myelin were engaged with Schwann cells in a 1:1 ratio (Fig. 5*A*). A subpopulation of these cells exhibited extended autophagic vacuoles containing degradative material reminiscent of myelin fragments (Fig. 5, *B* and *C*).

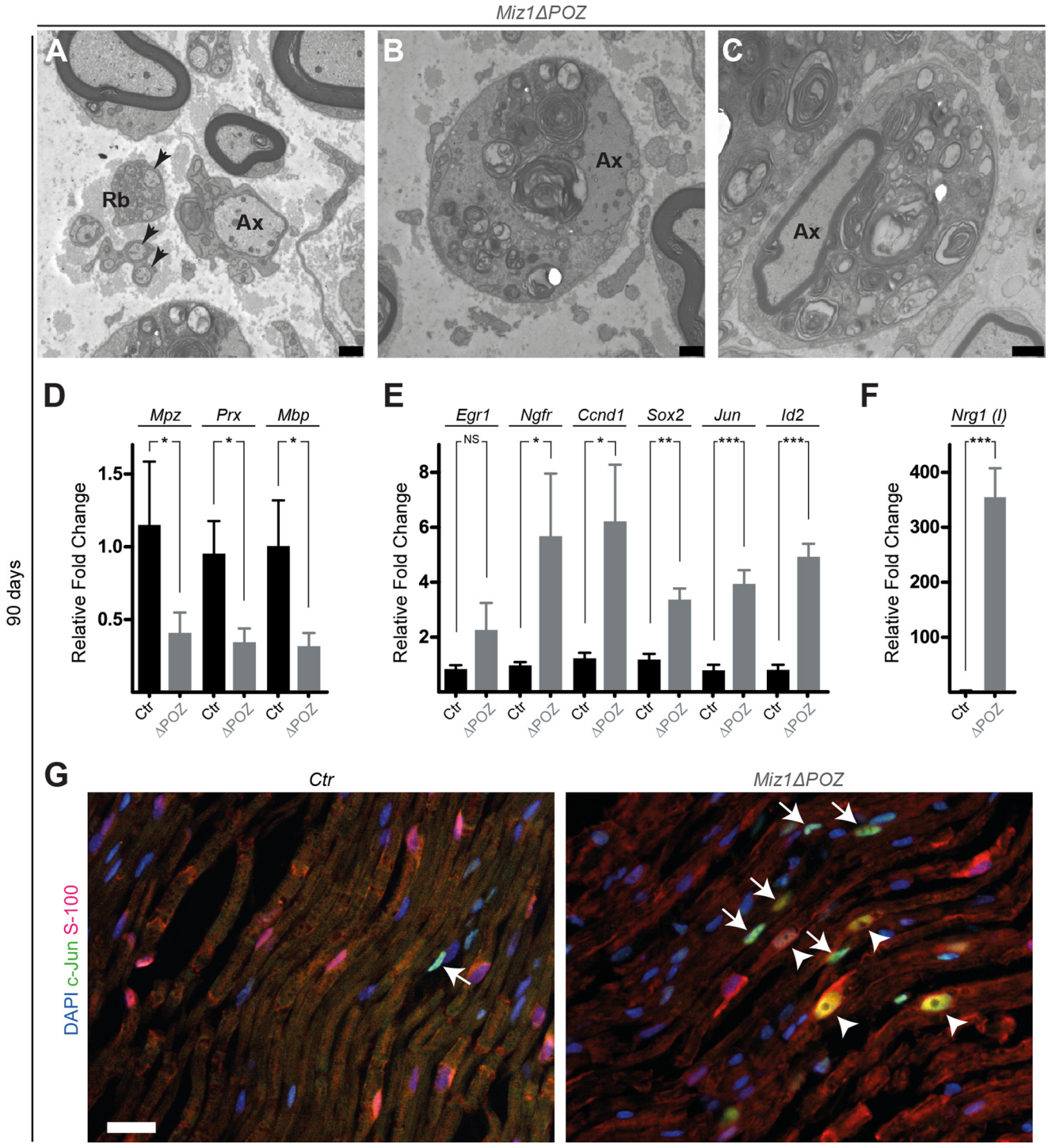

FIGURE 5. **Demyelination and dedifferentiation in sciatic nerve fibers from P90 *Miz1ΔPOZ* mice.** *A*, we observed Schwann cells associated with single large axons (*Ax*) lacking a myelin sheath. *Rb*, Remak bundle with unmyelinated axons (*arrowheads*). *B*, numerous autophagic vacuoles containing material reminiscent of myelin remnants were visible in some Schwann cells from *Miz1ΔPOZ* mice. In some of these Schwann cells, the axon was still surrounded by a myelin sheath (*C*), whereas in others, it was completely missing (*B*). *Ax*, axon. *D* and *E*, quantitative RT-PCR for the expression relative to GAPDH of the differentiation markers P0 (encoded by *Mpz*), periaxin (*Prx*), and myelin basic protein (*Mbp*) and for the dedifferentiation markers Krox24 (*Egr1*), p75 (*Ngfr*), cyclin D1 (*Ccnd1*), *Sox2*, c-*Jun*, and *Id2*. *F*, quantitative RT-PCR for Nrg1 (Type I). $n = 3$ mice per genotype, each run in triplicate. *G*, longitudinal sections of P90 sciatic nerve samples from *Miz1ΔPOZ* and control mice were co-stained with the Schwann cell marker S100 and c-Jun antibodies. Double-positive cells (*arrowheads*) were only detected in *Miz1ΔPOZ*, and c-Jun-only positive cells (*arrow*) were detectable in both conditions. *Bars*, 870 nm (*A* and *B*), 1000 nm (*C*), and 25 μm (*G*). *Error bars*, S.D. *, $p = 0.01–0.05$; **, $p = 0.001–0.01$; ***, $p < 0.001$; *NS*, not significant ($p > 0.05$).

To elucidate whether the loss of Miz1 POZ expression allowed dedifferentiation and remyelination, we determined the expression of differentiation and dedifferentiation markers at P90 by quantitative RT-PCR (20). We found that the expression of genes encoding differentiation markers, such as myelin protein zero (gene *Mpz*), periaxin (*Prx*), and myelin basic protein (*Mbp*), was significantly decreased in mutant sciatic nerves (Fig. 5*D*; $p < 0.05$). The expression of genes associated with

Schwann cell dedifferentiation, including *Ngfr*, *Ccnd1*, *Sox2*, c-*Jun*, and *Id2*, was clearly up-regulated in *Miz1*Δ*POZ* animals compared with age-matched controls (Fig. 5*E*). Because c-Jun is also highly expressed in macrophages (36) and because these invade the nerve (see below), we performed double immunofluorescence stainings with antibodies against c-Jun and the Schwann cell and neuronal marker S-100 (Fig. 5*G*). In control animals, only a few nuclei were positive for c-Jun, most of which were not correlated with the S-100 signal. In contrast, the number of c-Jun-positive nuclei increased in nerves from *Miz1*Δ*POZ* mice. Some of these positive nuclei were clearly located in Schwann cells, indicating that the increase of c-Jun expression is at least partly related to Schwann cells. The dedifferentiation marker Krox24 (encoded by the gene *Egr1*) was slightly but not significantly up-regulated (Fig. 5*E*; $p = 0.0670$). Furthermore, the expression of Schwann cell-derived neuregulin 1 (Type I), normally induced after adult nerve injury (37), was increased around 350-fold in 90-day-old knock-out sciatic nerves (Fig. 5*F*). In summary, ablation of the Miz1 POZ domain in Schwann cells induces myelin outfoldings and a late onset demyelination/dedifferentiation in 3-month-old mice, which can explain the motor disabilities of mutant mice already described.

Occasionally, we observed myelin-like structures in the interstitial space of 90-day-old *Miz1*Δ*POZ* nerves (Fig. 6*A*). Beside Schwann cells, we also found other cells with a pleiomorphic shape in the interstitial space (Fig. 6*B*). These cells also contained strongly degraded myelin-like material similar to what was observed in Schwann cells (compare with Fig. 5, *B* and *C*). When examined at higher magnification, these cells clearly lacked a basal lamina, whereas adjacent Schwann cells exhibited a continuous one (Fig. 6*C*). We hypothesized that cells competent for phagocytosis entered the sciatic nerve to clear myelin debris. Consistent with this notion was the focal increase of cells expressing the macrophage marker F4/80 antigen (Fig. 6*D*) (38) and an increase of *Emr1* expression, encoding F4/80 (Fig. 6*E*). Furthermore, quantitative PCR data (Fig. 6*F*) showed an increased expression of the cytokines *Ccl2* (macrophage chemoattractant protein 1; MCP-1), *Ccl3* (macrophage inflammatory protein 1α; Mip-1α), *Cxcl10* and *Cxcl14* (macrophage inflammatory protein 2γ; Mip-2γ), known as a potent monocyte chemoattractive substance, and of serum amyloid A1 and A2 (*Saa1* and *Saa2*) with multiple functions in inflammatory processes and acute phase responses (39, 40). However, neither by light nor by electron microscopy could we observe infiltration of lymphocytes or granulocytes. Also, the number of mast cells present in the nerve tissue did not differ between control and *Miz1*Δ*POZ* mice.

Phenotype in P200 to P300 Mice—Unexpectedly, the severe clinical symptoms visible in mutant mice of about 90–120 days of age disappeared in animals older than 120 days, although slight motor disabilities, such as a mild cramping of the hind legs, remained. This could be documented by motility score assessment. In P150 *Miz1*Δ*POZ* mice, the mean disability score was significantly lower than in P120 mice of this genotype, but it was still elevated compared with control animals (Fig. 2*B*). Furthermore, in the footprint assay, brush marks were no longer seen in P150 mice (Fig. 2*C*), and the strength of the forelimbs recovered to normal values (Fig. 2*D*).

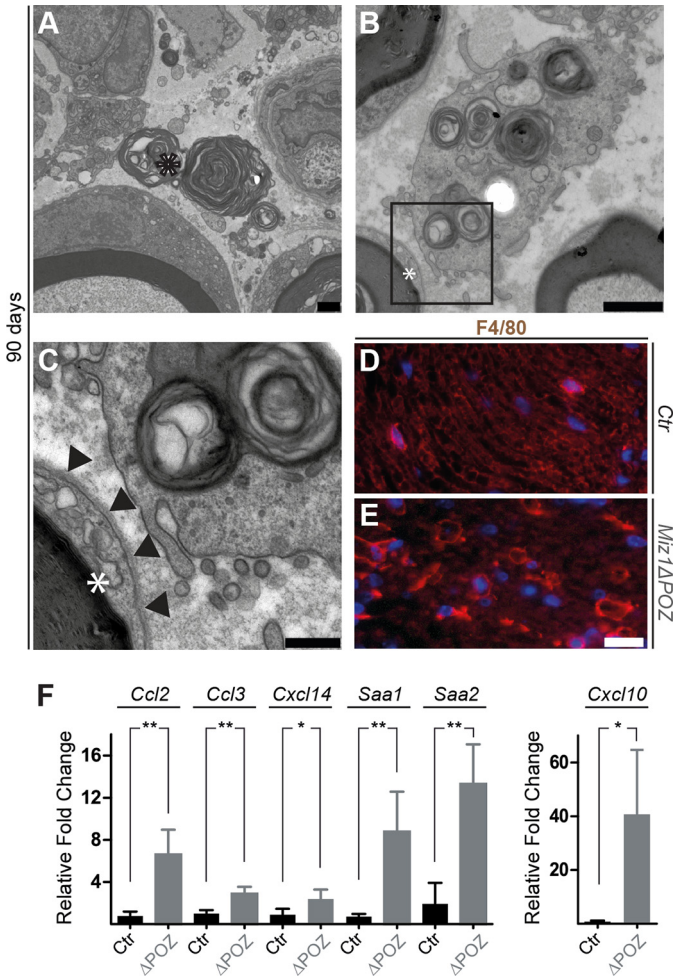

FIGURE 6. **P90 to P120 *Miz1*Δ*POZ* mice suffer from an inflammatory reaction.** *A*, we observed cell debris, including myelin-like structures (*asterisk*), in the interstitial space of *Miz1*Δ*POZ* mice. *B*, these structures were also found in cells with macrophage-like morphology. *Box*, region shown in *C*. *C*, at a higher magnification, macrophage-like cells did not exhibit a basement membrane, in contrast to an adjacent Schwann cell (*arrowheads*). *White asterisks* in *B* and *C* mark the same area. *D*, light microscopic sections stained with an antibody against the macrophage marker F4/80 and with Hoechst dye for nuclei. Positive cells in sciatic nerves from *Miz1*Δ*POZ* animals were focally distributed. *E*, quantitative RT-PCR for the expression of *Emr1* (encoding F4/80) relative to GAPDH in nerve tissue from P90 mice. *F*, quantitative RT-PCR for the expression relative to GAPDH of cytokines (*Ccl2*, *Ccl3*, *Cxcl10*, and *Cxcl14*) and acute phase markers (*Saa1* and *Saa2*) in nerve tissue from P90 mice. *Bars*, 1000 nm (*A* and *B*), 500 nm (*C*), and 50 μm (*D*). *Error bars*, S.D. *, $p = 0.01–0.05$; **, $p = 0.001–0.01$.

Consistently, electron microscopy revealed a persistent myelination phenotype in knock-out mice but with a decreased number and extension of outfoldings (4.2 ± 0.7%). Instead, a subpopulation of nerve fibers appeared to be remyelinated, as indicated by the presence of thin myelin sheets in relation to the diameter of the enwrapped axons (Fig. 7*A*). This observation was confirmed by a significantly increased g-ratio in sciatic nerves from *Miz1*Δ*POZ* mice (Fig. 7*E*) and a parallel shift of the regression lines in the scatter plot of axon to nerve fiber diameter (Fig. 7*F*). In addition, we identified earlier stages of remyelination in mutant nerves. We observed axons that were only touched and not enwrapped by Schwann cell processes (Fig.

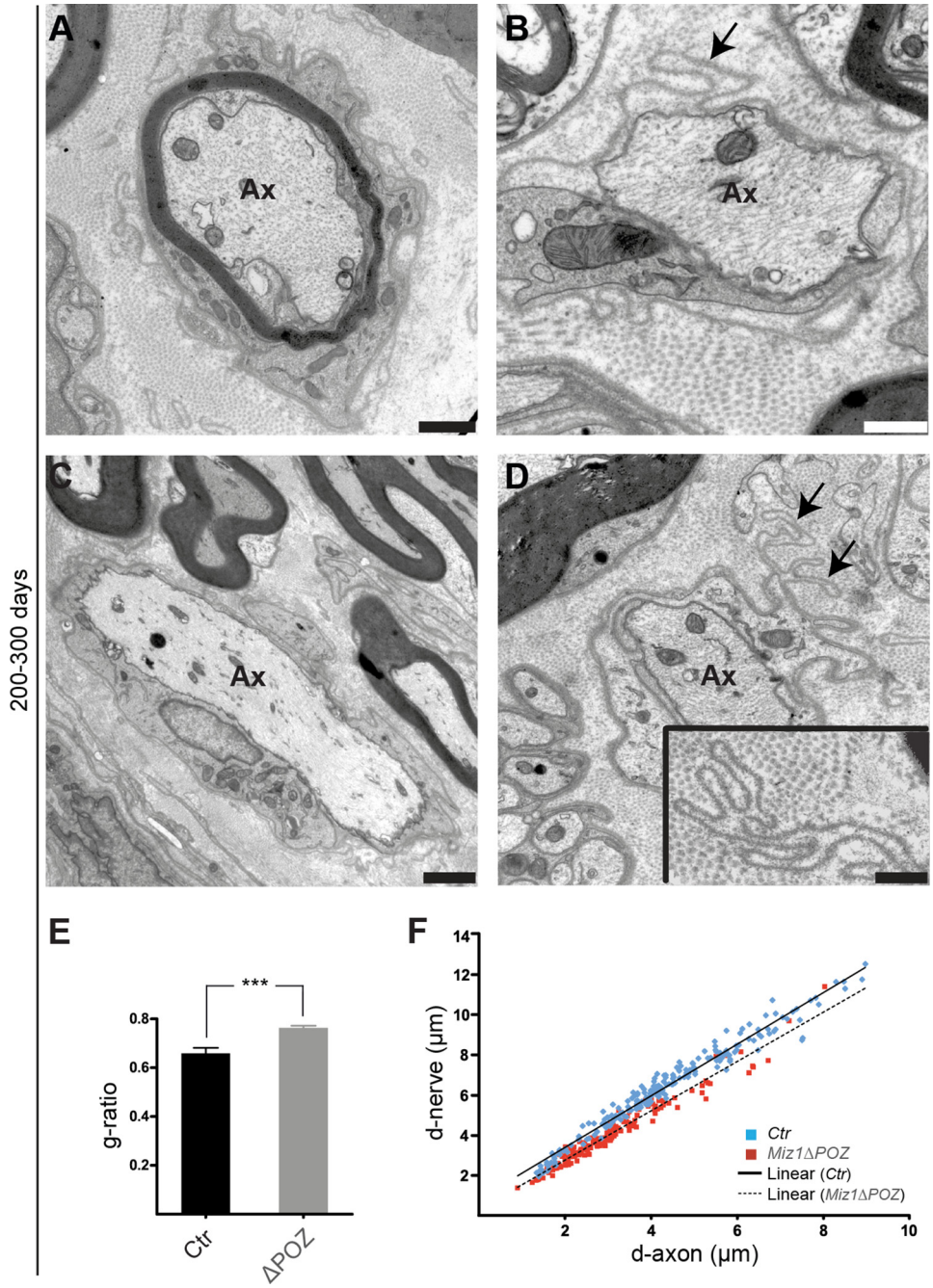

FIGURE 7. **Electron microscopy of sciatic nerves from P200 to P300 mice.** *A*, a considerable number of nerve fibers showed a thin myelin sheath in relation to the axon diameter. *B*, we observed large diameter axons that were only partially covered by Schwann cells. *C*, some axons of larger diameter were surrounded by Schwann cells that had not formed a myelin sheath. *D*, in addition, basement membranes that had detached from their Schwann cells were observed (*arrows* in *B* and *D*, *inset* in *D*). *E*, g-ratios of sciatic nerve fibers from control and *Miz1ΔPOZ* animals. ***, $p < 0.001$. *F*, scatter plot correlating the diameter of the axon to the diameter of the entire nerve fiber in sciatic nerves from control and *Miz1ΔPOZ* animals. *Bars*, 750 nm (*A*), 500 nm (*B*), 1500 nm (*C*), 750 nm (*D*), and 400 nm (*inset* in *D*). *Error bars*, S.D. ***, $p < 0.001$.

7*B*). Other axons of large diameter were surrounded by Schwann cells in a 1:1 ratio, but compact myelin had not yet been formed (Fig. 7*C*). Finally, we found basement membrane foldings not associated with cells, indicating that the corresponding Schwann cell had detached from this structure (Fig. 7, *B* and *D*). Taken together, these different structures suggest that demyelination and remyelination are processes ongoing simultaneously in *Miz1ΔPOZ* animals older than 120 days.

Analysis of serial block-faced microscopy stacks of images as well as conventional transmission electron microscopy revealed that some Schwann cells had lost their myelin completely (*e.g.* see Fig. 5*A*). The corresponding axon appeared darker and less granular, most likely due to changes of the neurofilament and microtubule cytoskeleton. Therefore, we co-stained sciatic nerves from P90 *Miz1ΔPOZ* and control mice with an antibody against unphosphorylated neurofilament-H from the SMI-32 clone and against neurofilament-M. SMI-32 positivity is a marker for degenerating axons, whereas the neurofilament-M antibody recognizes neurofilaments independently of the phosphorylation status (41, 42). Morpho-

metric quantifications uncovered no significant increase in SMI-32 signal intensity in *Miz1ΔPOZ* compared with control mice (Fig. 8*A*). In line with this observation was an unaltered pattern of succinate dehydrogenase staining in calf muscles of *Miz1ΔPOZ* mice at P90, P120, P150, P180, and P240, indicating that no sprouting had taken place (Fig. 8*B*).

Deletion of the Miz1 POZ Domain Affects Expression of Genes Involved in Myelin Homeostasis—A variety of Miz1 target genes, involved in vesicular transport, endocytosis, and autophagy, are down-regulated when the Miz1 POZ domain is deleted in Purkinje cells of the cerebellum and in mammary gland epithelial cells (10, 13). In line with this observation, the accumulation of polyubiquitinated proteins and p62 led to the hypothesis that Miz1 regulates the autophagic flux (10). Because myelin degradation also depends on autophagy (43, 44), we tested whether the expression of Miz1 target genes, encoding proteins relevant to vesicular transport and autophagy, is affected in Schwann cells of *Miz1ΔPOZ* mice. Among the 11 genes described previously (10, 13), only *Vamp4* was down-regulated, whereas *Pikfyve* and *Spast* were even more highly expressed (Fig. 9*A*). All other genes tested were not regulated, indicating that in Schwann cells, the deletion of the Miz1 POZ domain does not have the same impact on the expression of genes involved in vesicular transport and autophagy as has been described for Purkinje and mammary gland epithelial cells.

Myelin outfoldings similar to the pathology observed in *Miz1ΔPOZ* mice are characteristic histopathological features in a limited number of inherited peripheral neuropathies (45–50). The underlying pathomechanism has been attributed to dysregulated phosphoinositide levels and impaired vesicular transport (45, 46, 48, 50–52). We determined the expression of these genes by quantitative RT-PCR in *Miz1ΔPOZ* and *Ctr* mice. In addition, we chose genes encoding proteins that interact with the proteins associated with these disease genes. We found an altered expression of *Mtmr2* (myotubularin-related protein 2), *Mtmr7*, *Mtmr9*, *Fdg4* (FYVE/RhoGEF/PH domain-containing 4), *Dlg1* (discs large homolog 1), *Pten* (phosphatase and tensin homolog), and *Exoc4* (exocyst complex component 4). However, except for *Mtmr7*, all of these genes were expressed on a higher level when the Miz1 POZ domain was deleted (Fig. 9*B*), most likely secondarily due to the dysmyelination. Our data suggest that neither previously identified Miz targets involved in vesicular transport and autophagy nor genes related to peripheral neuropathies with similar histopathologic changes are likely to be causative for the phenotype observed in *Miz1ΔPOZ* mice.

Deletion of the Miz1 POZ Domain Induces a Senescence-like Phenotype in Schwann Cells—Ablation of the Miz1 POZ domain in keratinocytes leads to an increased expression of the cyclin- dependent kinase inhibitor $p21^{Cip1}$ due to a relieved repression of *Cdkn1a* via functional Myc-Miz1 complexes (12). $p21^{Cip1}$ is also up-regulated in Schwann cells following a nerve injury (19). Quantitative RT-PCR together with immunohistochemical stainings of sciatic nerves from P90 mice revealed a strong up-regulation of $p21^{Cip1}$ in Schwann cells from *Miz1ΔPOZ* animals compared with age-matched controls (Fig. 10, *A* and *B*). Staining for the proliferation marker Ki67 revealed

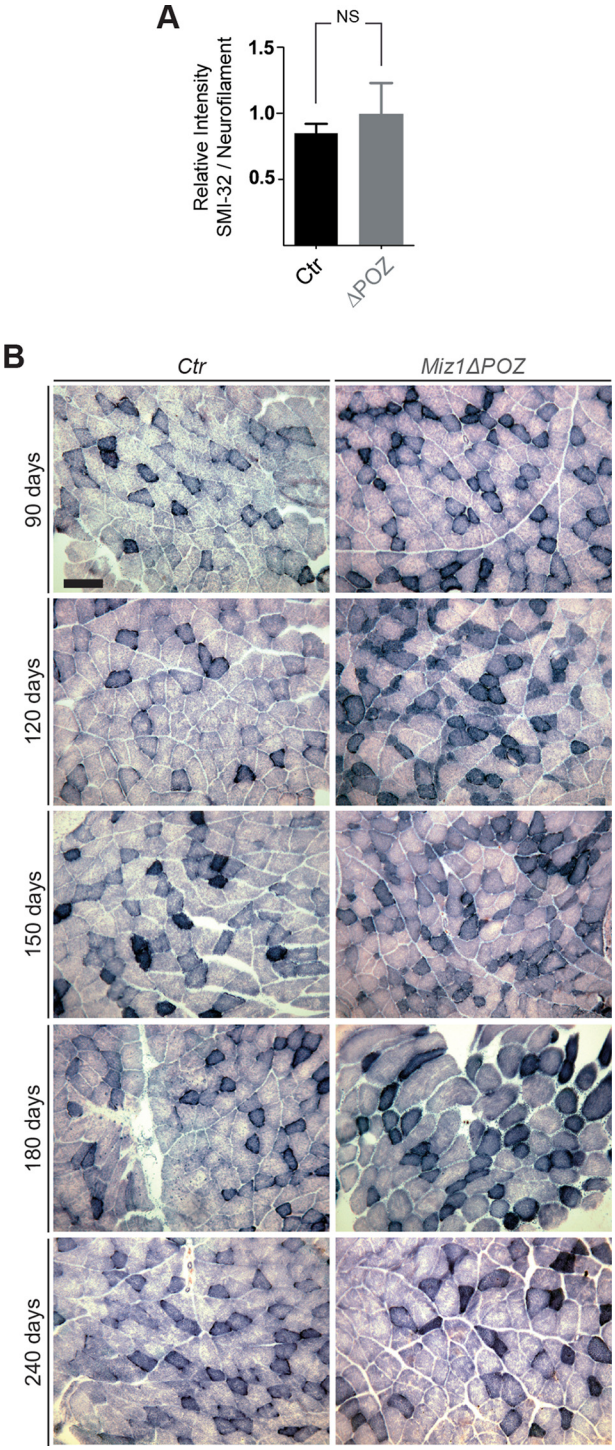

FIGURE 8. **No axonal degeneration or sprouting in aged *Miz1ΔPOZ* mice.** *A*, longitudinal sections of sciatic nerves from 90-day-old *Miz1ΔPOZ* and control mice were stained with a neurofilament-M antibody to detect neurofilaments independent of the phosphorylation status and with SMI-32 to detect unphosphorylated neurofilament-H. No differences were detected, comparing the staining pattern and intensities in *Miz1ΔPOZ* and control mice. To determine the ratio of SMI-32 in relation to the neurofilament-M signals, the fluorescent intensities were quantified on three independent pictures per animal. The graph depicts the relative intensities of four controls and four *Miz1ΔPOZ* animals represented as mean and S.D. ($n = 4$). *B*, histochemical staining of succinate dehydrogenase in calf muscles from P90, P120, P150, P180, and P240 *Ctr* and *Miz1ΔPOZ* mice. *Bar*, 100 μm. *Error bars*, S.D. *NS*, not significant ($p > 0.05$).

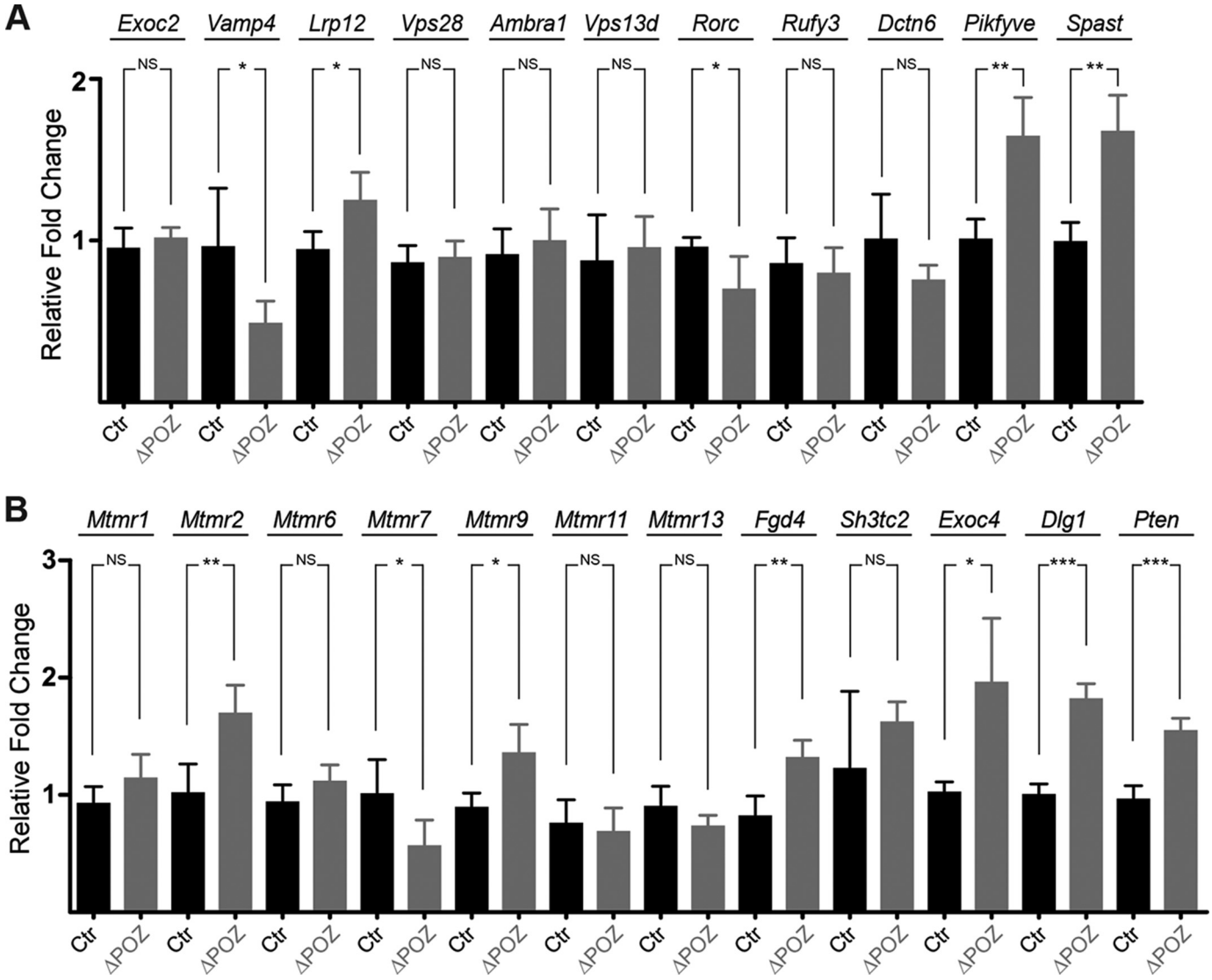

FIGURE 9. **Genes annotated to vesicular traffic or myelin outfoldings are not down-regulated in *Miz1ΔPOZ* mice.** Expression of Miz1 direct target genes (*A*) and of genes involved in myelin homeostasis (*B*) is shown. *Error bars*, S.D. *, $p = 0.01–0.05$; **, $p = 0.001–0.01$; ***, $p < 0.001$; *NS*, not significant ($p > 0.05$).

a 5-fold higher labeling index in nerve tissue from *Miz1ΔPOZ* mice compared with control animals, and this was confirmed by changes in the expression of *Mki67* (Fig. 10*C*). Because $p21^{Cip1}$ expression inhibits cell cycle progression (53), we performed immunohistochemical staining of Ki67 and the macrophage marker F4/80 to unravel the identity of the proliferating cells in the tissue. Most Ki67-positive cells also expressed F4/80 (Fig. 10*D*), indicating that the increased Ki67 labeling index is mainly related to the proliferation of macrophages.

Besides its role in cell cycle regulation, $p21^{Cip1}$ has been identified as a crucial player in the establishment and maintenance of senescence (54, 55). To this end, we prepared sciatic nerve fragments and performed whole-mount SA β-galactosidase staining to probe for this senescence marker (13). Nerve fragments from *Miz1ΔPOZ* mice were, in contrast to those from controls, positive for SA β-galactosidase, albeit to a variable extent (Fig. 10*E*). In addition, we used an antibody against the senescence-associated H3K9me3 (56) and found a higher percentage of positive Schwann cell nuclei in *Miz1ΔPOZ* animals compared with control animals (Fig. 10, *F* and *G*).

DISCUSSION

Ablation of the Miz1 POZ domain in Schwann cells did not affect the establishment of myelination but was followed at around 3 months of age by demyelination, as observed in sciatic nerve fibers. This was associated with motor constraints of knock-out mice. These motor disabilities were first observed around P90 and were accompanied by features of dys- and demyelination, such as myelin outfoldings, tomacula, and degradation of myelin by Schwann cells and invading macrophages with a severity ranging to complete loss of myelin sheets around axons. Interestingly, careful ultrastructural analysis and determination of the g-ratio in sciatic nerves from P30 *Miz1ΔPOZ* mice revealed no abnormalities when compared with tissue from control animals, although *Miz1* is expressed in Schwann cell nuclei already at P10. We conclude that Miz1 is not necessary for the development of myelin sheets and that the de- and dysmyelinating processes are initiated between P30 and P90. Late onset neuropathies in a similar time range have been described in other animal models. However, most of these

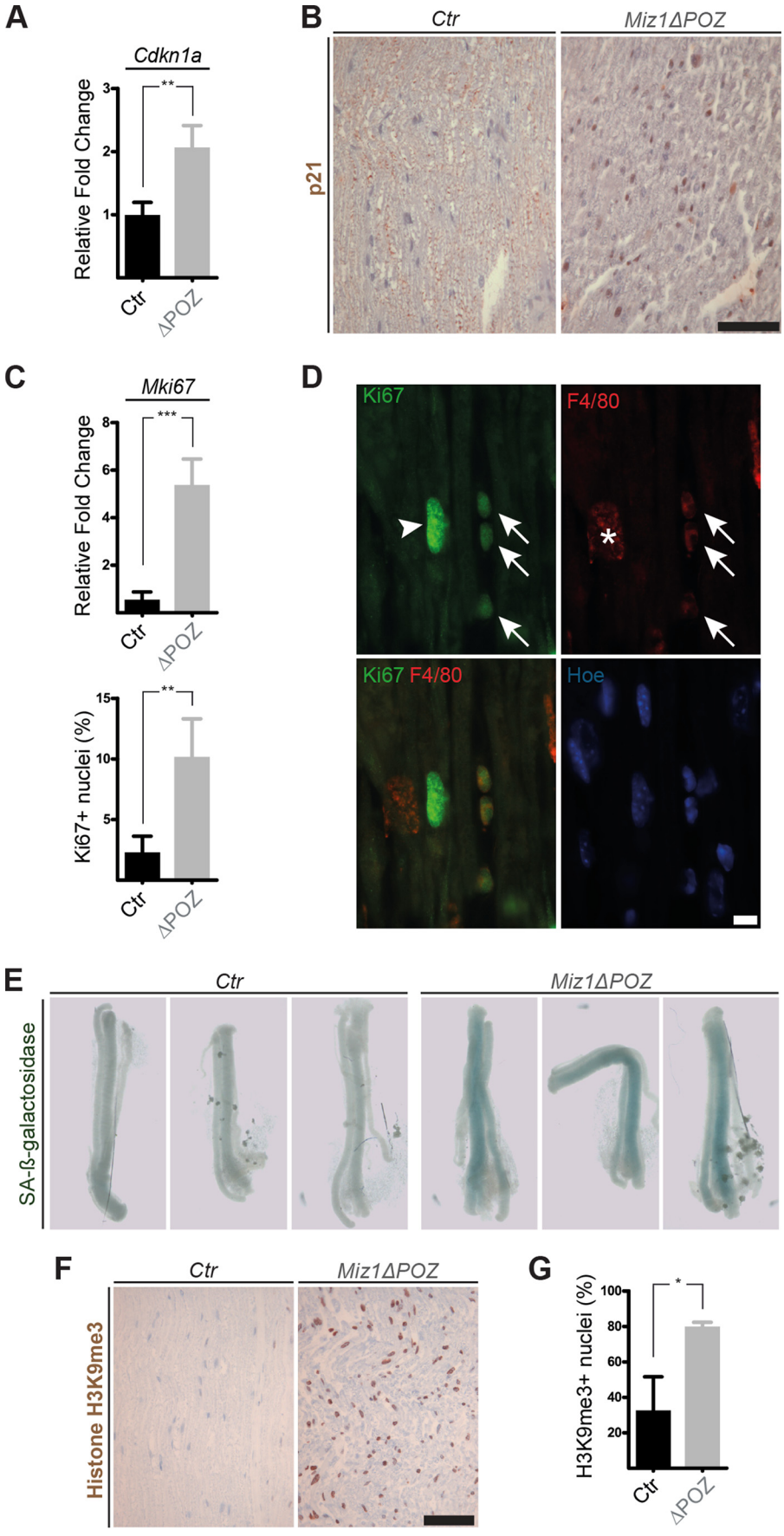
A
Cdkn1a
Relative Fold Change
**
Ctr
ΔPOZ
B
Ctr
Miz1ΔPOZ
p21
C
Mki67
Relative Fold Change
***
Ctr
ΔPOZ
Ki67+ nuclei (%)
**
Ctr
ΔPOZ
D
Ki67
F4/80
Ki67 F4/80
Hoe
E
Ctr
Miz1ΔPOZ
SA-ß-galactosidase
F
Ctr
Miz1ΔPOZ
Histone H3K9me3
G
H3K9me3+ nuclei (%)
*
Ctr
ΔPOZ

models mimicking analogous neuropathies are progressive in the development of their phenotype (57, 58). In *Miz1*Δ*POZ* animals, the neuropathic symptoms observed were reduced starting from the age of 120 days. In P200 knock-out mice, motor disabilities were hardly observable, indicating that the peripheral nervous tissue spontaneously regenerated. Ultrastructural analysis of knock-out sciatic nerves at this time point revealed that the number of outfoldings decreased, although tomacula were regularly observed and most axons were hypomyelinated, which was also reflected by an increased g-ratio. Our observations suggest that after initiation of an acute neuropathy at 3 months of age, regenerative processes are activated to compensate for the damage to peripheral nerve tissue. The increased expression of genes, such as *Mtmr2*, *Mtmr9*, *Exoc4*, *Dgl1*, *Fdg4*, or *Pten*, all involved in myelin homeostasis (45, 46), also underlines the notion of a regenerative process. Although the myelination is not completely restored even at P200, ongoing damage and regeneration could be counterbalanced in such a way that the motor abilities of *Miz1*Δ*POZ* mice are almost normal.

The development of a late onset phenotype followed by its remission was unexpected because the loss of function mutation in Miz1 was induced at embryonic day 12 in the Schwann cell lineage and thus is also present in the remyelinating Schwann cells. The results demonstrate that Miz1 function is neither needed for myelin formation in development, which is completed around P30 (15), nor for regeneration. Based on the presented data, we suggest that loss of a functional Miz1 could interfere with normally suppressed pathways that promote demyelination. Consistently, we found that the expression of negative regulators of myelination, including c-Jun, Sox2, and Id2, was significantly up-regulated in *Miz1*Δ*POZ* mice (Fig. 5*E*). Following nerve injury, c-Jun, Sox2, and Id2 are crucial for adaptation of Schwann cells because they promote a transdifferentiation to an immature type of Schwann cells (36, 59). However, other pathways driving demyelination, such as the Ras/Raf/MEK/ERK pathway (20), were not up-regulated in *Miz1*Δ*POZ* mice (data not shown). This demonstrates that the tissue damage observed in *Miz1*Δ*POZ* sciatic nerves does not lead to a general up-regulation of dedifferentiation factors and supports the hypothesis that the up-regulation of c-Jun, Id2, and Sox2 could play a central role in the pathology of *Miz1*Δ*POZ* mice. Interestingly, Miz1 has been shown to inhibit TNFα-dependent activation of c-Jun N-terminal kinase (JNK1) (60), which in turn activates c-Jun. The loss of a functional Miz1 could promote c-Jun activation by relieving Jnk1 inhibition; ongoing experiments test this hypothesis.

As shown in Fig. 5*D*, the expression of myelin protein zero (P0), periaxin, or myelin basic protein is decreased in P90 *Miz1*Δ*POZ* sciatic nerves compared with controls. This is underscored by a simultaneous increase in the expression of genes encoding proteins such as Krox24, p75, or cyclin D1, which promote the transition of Schwann cells back to a promyelinating state (15, 61), and by a dramatic increase of neuregulin 1 (type I) as an indicator of disturbed Schwann cell/axon interaction (37). It is also conceivable that a direct down-regulation of the expression of *Pmp22* (as observed in our preliminary DNA array data) or one of the other structural myelin proteins mentioned earlier could be the initial trigger for the phenotype observed after Miz1 POZ domain ablation, similar to the dose-dependent onset in Pmp22-induced peripheral neuropathy models (62, 63). However, a direct binding of Miz1 to genes encoding myelin proteins remains to be elucidated.

Recently, a function of Miz1 in the regulation of autophagy has been described in Purkinje cells based on a correlation between genes to which Miz1 binds and their down-regulation in *Nestin-Cre Miz1*Δ*POZ* mice. Many of these genes are important for vesicular transport in general or autophagy in particular (10). Similar results were recently obtained using primary mammary cells from control and *Miz1*Δ*POZ* lactating glands (13). In Schwann cells, autophagic removal of myelin debris after nerve damage has been described (43). Additionally, myelin debris can be cleared by macrophages (44). However, among the known Miz1 target genes associated with autophagy (10, 13), only the expression of Vamp4 was reduced in nerve tissue from *Miz1*Δ*POZ* mice; two genes were even more strongly expressed, and all others were not regulated. This indicates that a loss of expression of the tested genes associated with autophagy is not likely to be causative for the observed phenotype.

After the discovery of Miz1 as a Myc-binding protein, the favored model saw the Miz1-Myc complex as a repressor of gene expression (64, 65). This was originally shown in cell culture for the cyclin-dependent kinase inhibitor gene *Cdkn2b*, encoding $p15^{INK4b}$ (28, 66), and was extended to a variety of other genes (13, 54). The repressive function of the Miz1-Myc complex was confirmed, especially for *Cdkn1a* (encoding $p21^{Cip1}$), in keratinocytes *in vivo* (11). In line with this model, skin tumorigenesis is attenuated in mice with a Miz1 POZ domain ablation in keratinocytes through an increased $p21^{Cip1}$ expression, which inhibits proliferation and increases the expression of SA β-galactosidase (12). Schwann cells from 90-day-old *Miz1*Δ*POZ* animals also have elevated levels of $p21^{Cip1}$ when compared with those from control mice, where $p21^{Cip1}$ was hardly detected. Interestingly, nerve injury also leads to a nuclear accumulation of $p21^{Cip1}$ (19), indicating that an increase in $p21^{Cip1}$ expression can be a common reaction of Schwann cells to diverse types of damage. Besides its role in the cell cycle, $p21^{Cip1}$ is involved in other cellular processes, including regulation of the actin cytoskeleton, apoptosis, and senescence (67). The expression of SA β-galactosidase and the high amount of H3K9me3 in *Miz1*Δ*POZ* sciatic nerves are reminis-

FIGURE 10. **Expression of senescence and proliferation markers in sciatic nerves of P90 *Miz1*Δ*POZ* mice.** *A*, expression of *Cdkn1a* (encoding $p21^{Cip1}$), obtained by quantitative RT-PCR. *B*, immunostaining of the cyclin-dependent kinase inhibitor $p21^{Cip1}$ in nerve tissue from *Ctr* and *Miz1*Δ*POZ* animals. *C*, expression of *Mki67* (encoding Ki67), obtained by quantitative RT-PCR, and Ki67 labeling index. *D*, double immunofluorescence staining with an antibody against the macrophage marker protein F4/80 and against Ki67. *E*, histochemical whole-mount staining of the SA β-galactosidase was negative in control nerve fragments (*top row*) but positive in *Miz1*Δ*POZ* animals (*bottom row*). *F*, immunostaining with an antibody against the senescence-related H3K9me3 in sciatic nerve tissue from *Ctr* and *Miz1*Δ*POZ* mice. *G*, H3K9me3 labeling index. *Arrows*, cells positive for Ki67 and F4/80; *arrowhead*, cell positive only for Ki67. *Bars*, 50 μm (*B* and *F*) and 20 μm (*D*). *Error bars*, S.D. *, $p = 0.01–0.05$; **, $p = 0.001–0.01$; ***, $p < 0.001$.

cent of cellular senescence. This can also be induced by $p21^{Cip1}$ (54), although the detailed molecular link between this protein and senescence is still obscure (67). According to these findings and our data, we propose that the deletion of the Miz1 POZ domain in Schwann cells leads to a premature cellular senescence, which might be a direct cause of the up-regulation of the Miz1 target gene *Cdkn1a*.

Acknowledgments—The expert technical assistance of Waltraud Ackermann, Claudia Mayrhofer, Ursula Lehr, and Brigitte Agricola is gratefully acknowledged. We thank Burkhard Schütz for the device to measure grip strength. We thank Klaus V. Toyka and Carsten Wessig for helpful discussions and Ned Mantei for carefully reading the manuscript.

REFERENCES

1. Peukert, K., Staller, P., Schneider, A., Carmichael, G., Hänel, F., and Eilers, M. (1997) An alternative pathway for gene regulation by Myc. *EMBO J.* **16,** 5672–5686
2. Kosan, C., Saba, I., Godmann, M., Herold, S., Herkert, B., Eilers, M., and Möröy, T. (2010) Transcription factor miz-1 is required to regulate interleukin-7 receptor signaling at early commitment stages of B cell differentiation. *Immunity* **33,** 917–928
3. Möröy, T., Saba, I., and Kosan, C. (2011) The role of the transcription factor Miz-1 in lymphocyte development and lymphomagenesis: binding Myc makes the difference. *Semin. Immunol.* **23,** 379–387
4. Stead, M. A., and Wright, S. C. (2014) Nac1 interacts with the POZ-domain transcription factor, Miz1. *Biosci. Rep.* 10.1042/BSR20140049
5. Stogios, P. J., Downs, G. S., Jauhal, J. J. S., Nandra, S. K., and Privé, G. G. (2005) Sequence and structural analysis of BTB domain proteins. *Genome Biol.* **6,** R82
6. Herkert, B., and Eilers, M. (2010) Transcriptional repression: the dark side of myc. *Genes Cancer* **1,** 580–586
7. Adhikary, S., Peukert, K., Karsunky, H., Beuger, V., Lutz, W., Elsässer, H.-P., Möröy, T., and Eilers, M. (2003) Miz1 is required for early embryonic development during gastrulation. *Mol. Cell. Biol.* **23,** 7648–7657
8. Kerosuo, L., Piltti, K., Fox, H., Angers-Loustau, A., Häyry, V., Eilers, M., Sariola, H., and Wartiovaara, K. (2008) Myc increases self-renewal in neural progenitor cells through Miz-1. *J. Cell Sci.* **121,** 3941–3950
9. Lein, E. S., Hawrylycz, M. J., Ao, N., Ayres, M., Bensinger, A., Bernard, A., Boe, A. F., Boguski, M. S., Brockway, K. S., Byrnes, E. J., Chen, L., Chen, L., Chen, T.-M., Chin, M. C., Chong, J., Crook, B. E., Czaplinska, A., Dang, C. N., Datta, S., Dee, N. R., Desaki, A. L., Desta, T., Diep, E., Dolbeare, T. A., Donelan, M. J., Dong, H.-W., Dougherty, J. G., Duncan, B. J., Ebbert, A. J., Eichele, G., Estin, L. K., Faber, C., Facer, B. A., Fields, R., Fischer, S. R., Fliss, T. P., Frensley, C., Gates, S. N., Glattfelder, K. J., Halverson, K. R., Hart, M. R., Hohmann, J. G., Howell, M. P., Jeung, D. P., Johnson, R. A., Karr, P. T., Kawal, R., Kidney, J. M., Knapik, R. H., Kuan, C. L., Lake, J. H., Laramee, A. R., Larsen, K. D., Lau, C., Lemon, T. A., Liang, A. J., Liu, Y., Luong, L. T., Michaels, J., Morgan, J. J., Morgan, R. J., Mortrud, M. T., Mosqueda, N. F., Ng, L. L., Ng, R., Orta, G. J., Overly, C. C., Pak, T. H., Parry, S. E., Pathak, S. D., Pearson, O. C., Puchalski, R. B., Riley, Z. L., Rockett, H. R., Rowland, S. A., Royall, J. J., Ruiz, M. J., Sarno, N. R., Schaffnit, K., Shapovalova, N. V., Sivisay, T., Slaughterbeck, C. R., Smith, S. C., Smith, K. A., Smith, B. I., Sodt, A. J., Stewart, N. N., Stumpf, K.-R., Sunkin, S. M., Sutram, M., Tam, A., Teemer, C. D., Thaller, C., Thompson, C. L., Varnam, L. R., Visel, A., Whitlock, R. M., Wohnoutka, P. E., Wolkey, C. K., Wong, V. Y., Wood, M., Yaylaoglu, M. B., Young, R. C., Youngstrom, B. L., Feng Yuan, X., Zhang, B., Zwingman, T. A., and Jones, A. R. (2007) Genome-wide atlas of gene expression in the adult mouse brain. *Nature* **445,** 168–176
10. Wolf, E., Gebhardt, A., Kawauchi, D., Walz, S., von Eyss, B., Wagner, N., Renninger, C., Krohne, G., Asan, E., Roussel, M. F., and Eilers, M. (2013) Miz1 is required to maintain autophagic flux. *Nat. Commun.* **4,** 2535
11. Gebhardt, A., Kosan, C., Herkert, B., Möröy, T., Lutz, W., Eilers, M., and Elsässer, H.-P. (2007) Miz1 is required for hair follicle structure and hair morphogenesis. *J. Cell Sci.* **120,** 2586–2593
12. Hönnemann, J., Sanz-Moreno, A., Wolf, E., Eilers, M., and Elsässer, H.-P. (2012) Miz1 is a critical repressor of cdkn1a during skin tumorigenesis. *PloS One* **7,** e34885
13. Sanz-Moreno, A., Fuhrmann, D., Wolf, E., von Eyss, B., Eilers, M., and Elsässer, H.-P. (2014) Miz1 deficiency in the mammary gland causes a lactation defect by attenuated Stat5 expression and phosphorylation. *PLoS ONE* **9,** e89187
14. Mirsky, R., Woodhoo, A., Parkinson, D. B., Arthur-Farraj, P., Bhaskaran, A., and Jessen, K. R. (2008) Novel signals controlling embryonic Schwann cell development, myelination and dedifferentiation. *J. Peripher. Nerv. Syst.* **13,** 122–135
15. Svaren, J., and Meijer, D. (2008) The molecular machinery of myelin gene transcription in Schwann cells. *Glia* **56,** 1541–1551
16. Woodhoo, A., and Sommer, L. (2008) Development of the Schwann cell lineage: from the neural crest to the myelinated nerve. *Glia* **56,** 1481–1490
17. Bosse, F. (2012) Extrinsic cellular and molecular mediators of peripheral axonal regeneration. *Cell Tissue Res.* **349,** 5–14
18. Martini, R., Klein, D., and Groh, J. (2013) Similarities between inherited demyelinating neuropathies and Wallerian degeneration: an old repair program may cause myelin and axon perturbation under nonlesion conditions. *Am. J. Pathol.* **183,** 655–660
19. Atanasoski, S., Boller, D., De Ventura, L., Koegel, H., Boentert, M., Young, P., Werner, S., and Suter, U. (2006) Cell cycle inhibitors p21 and p16 are required for the regulation of Schwann cell proliferation. *Glia* **53,** 147–157
20. Napoli, I., Noon, L. A., Ribeiro, S., Kerai, A. P., Parrinello, S., Rosenberg, L. H., Collins, M. J., Harrisingh, M. C., White, I. J., Woodhoo, A., and Lloyd, A. C. (2012) A central role for the ERK-signaling pathway in controlling Schwann cell plasticity and peripheral nerve regeneration *in vivo*. *Neuron* **73,** 729–742
21. Harrisingh, M. C., Perez-Nadales, E., Parkinson, D. B., Malcolm, D. S., Mudge, A. W., and Lloyd, A. C. (2004) The Ras/Raf/ERK signalling pathway drives Schwann cell dedifferentiation. *EMBO J.* **23,** 3061–3071
22. Gorgoulis, V. G., and Halazonetis, T. D. (2010) Oncogene-induced senescence: the bright and dark side of the response. *Curr. Opin. Cell Biol.* **22,** 816–827
23. Serrano, M., Lin, A. W., McCurrach, M. E., Beach, D., and Lowe, S. W. (1997) Oncogenic ras provokes premature cell senescence associated with accumulation of p53 and p16INK4a. *Cell* **88,** 593–602
24. Jaegle, M., Ghazvini, M., Mandemakers, W., Piirsoo, M., Driegen, S., Levavasseur, F., Raghoenath, S., Grosveld, F., and Meijer, D. (2003) The POU proteins Brn-2 and Oct-6 share important functions in Schwann cell development. *Genes Dev.* **17,** 1380–1391
25. King, R. H., Craggs, R. I., Gross, M. L., Tompkins, C., and Thomas, P. K. (1983) Suppression of experimental allergic neuritis by Cyclosporin-A. *Acta Neuropathol.* **59,** 262–268
26. Carter, R. J., Lione, L. A., Humby, T., Mangiarini, L., Mahal, A., Bates, G. P., Dunnett, S. B., and Morton, A. J. (1999) Characterization of progressive motor deficits in mice transgenic for the human Huntington's disease mutation. *J. Neurosci.* **19,** 3248–3257
27. Bremer, J., Baumann, F., Tiberi, C., Wessig, C., Fischer, H., Schwarz, P., Steele, A. D., Toyka, K. V., Nave, K.-A., Weis, J., and Aguzzi, A. (2010) Axonal prion protein is required for peripheral myelin maintenance. *Nat. Neurosci.* **13,** 310–318
28. Staller, P., Peukert, K., Kiermaier, A., Seoane, J., Lukas, J., Karsunky, H., Möröy, T., Bartek, J., Massagué, J., Hänel, F., and Eilers, M. (2001) Repression of p15INK4b expression by Myc through association with Miz-1. *Nat. Cell Biol.* **3,** 392–399
29. Ito, S., and Karnovsky, M. J. (1968) Formaldehyde-glutaraldehyde fixatives containing trinitro compounds. *J. Cell Biol.* **39,** 168a–169a
30. Denk, W., and Horstmann, H. (2004) Serial block-face scanning electron microscopy to reconstruct three-dimensional tissue nanostructure. *PLoS Biol.* **2,** e329
31. Zankel, A., Kraus, B., Poelt, P., Schaffer, M., and Ingolic, E. (2009) Ultramicrotomy in the ESEM, a versatile method for materials and life sciences. *J. Microsc.* **233,** 140–148

32. Lindeboom, F., Gillemans, N., Karis, A., Jaegle, M., Meijer, D., Grosveld, F., and Philipsen, S. (2003) A tissue-specific knockout reveals that Gata1 is not essential for Sertoli cell function in the mouse. *Nucleic Acids Res.* **31,** 5405–5412
33. Joseph, N. M., Mukouyama, Y.-S., Mosher, J. T., Jaegle, M., Crone, S. A., Dormand, E.-L., Lee, K.-F., Meijer, D., Anderson, D. J., and Morrison, S. J. (2004) Neural crest stem cells undergo multilineage differentiation in developing peripheral nerves to generate endoneurial fibroblasts in addition to Schwann cells. *Development* **131,** 5599–5612
34. Hartung, H.-P., Schäfer, B., Heininger, K., Stoll, G., and Toyka, K. V. (1988) The role of macrophages and eicosanoids in the pathogenesis of experimental allergic neuritis serial clinical, electrophysiological, biochemical and morphological observations. *Brain* **111,** 1039–1059
35. Yang, M., Rainone, A., Shi, X. Q., Fournier, S., and Zhang, J. (2014) A new animal model of spontaneous autoimmune peripheral polyneuropathy: implications for Guillain-Barré syndrome. *Acta Neuropathol. Commun.* **2,** 5
36. Arthur-Farraj, P. J., Latouche, M., Wilton, D. K., Quintes, S., Chabrol, E., Banerjee, A., Woodhoo, A., Jenkins, B., Rahman, M., Turmaine, M., Wicher, G. K., Mitter, R., Greensmith, L., Behrens, A., Raivich, G., Mirsky, R., and Jessen, K. R. (2012) c-Jun reprograms Schwann cells of injured nerves to generate a repair cell essential for regeneration. *Neuron* **75,** 633–647
37. Stassart, R. M., Fledrich, R., Velanac, V., Brinkmann, B. G., Schwab, M. H., Meijer, D., Sereda, M. W., and Nave, K.-A. (2013) A role for Schwann cell-derived neuregulin-1 in remyelination. *Nat. Neurosci.* **16,** 48–54
38. Khazen, W., M'bika, J.-P., Tomkiewicz, C., Benelli, C., Chany, C., Achour, A., and Forest, C. (2005) Expression of macrophage-selective markers in human and rodent adipocytes. *FEBS Lett.* **579,** 5631–5634
39. Cray, C., Zaias, J., and Altman, N. H. (2009) Acute phase response in animals: a review. *Comp. Med.* **59,** 517–526
40. Eklund, K. K., Niemi, K., and Kovanen, P. T. (2012) Immune functions of serum amyloid A. *Crit. Rev. Immunol.* **32,** 335–348
41. Meller, D., Eysel, U. T., and Schmidt-Kastner, R. (1994) Transient immunohistochemical labelling of rat retinal axons during Wallerian degeneration by a monoclonal antibody to neurofilaments. *Brain Res.* **648,** 162–166
42. Roussarie, J.-P., Ruffié, C., Edgar, J. M., Griffiths, I., and Brahic, M. (2007) Axon myelin transfer of a non-enveloped virus. *PloS One* **2,** e1331
43. Holtzman, E., and Novikoff, A. B. (1965) Lysosomes in the rat sciatic nerve following crush. *J. Cell Biol.* **27,** 651–669
44. Perry, V. H., Tsao, J. W., Fearn, S., and Brown, M. C. (1995) Radiation-induced reductions in macrophage recruitment have only slight effects on myelin degeneration in sectioned peripheral nerves of mice. *Eur. J. Neurosci.* **7,** 271–280
45. Pereira, J. A., Lebrun-Julien, F., and Suter, U. (2012) Molecular mechanisms regulating myelination in the peripheral nervous system. *Trends Neurosci.* **35,** 123–134
46. Niemann, A., Berger, P., and Suter, U. (2006) Pathomechanisms of mutant proteins in Charcot-Marie-Tooth disease. *Neuromolecular Med.* **8,** 217–242
47. Bolis, A., Coviello, S., Bussini, S., Dina, G., Pardini, C., Previtali, S. C., Malaguti, M., Morana, P., Del Carro, U., Feltri, M. L., Quattrini, A., Wrabetz, L., and Bolino, A. (2005) Loss of Mtmr2 phosphatase in Schwann cells but not in motor neurons causes Charcot-Marie-Tooth type 4B1 neuropathy with myelin outfoldings. *J. Neurosci.* **25,** 8567–8577
48. Bolis, A., Coviello, S., Visigalli, I., Taveggia, C., Bachi, A., Chishti, A. H., Hanada, T., Quattrini, A., Previtali, S. C., Biffi, A., and Bolino, A. (2009) Dlg1, Sec8, and Mtmr2 regulate membrane homeostasis in Schwann cell myelination. *J. Neurosci.* **29,** 8858–8870
49. Tersar, K., Boentert, M., Berger, P., Bonneick, S., Wessig, C., Toyka, K. V., Young, P., and Suter, U. (2007) Mtmr13/Sbf2-deficient mice: an animal model for CMT4B2. *Hum. Mol. Genet.* **16,** 2991–3001
50. Horn, M., Baumann, R., Pereira, J. A., Sidiropoulos, P. N. M., Somandin, C., Welzl, H., Stendel, C., Lühmann, T., Wessig, C., Toyka, K. V., Relvas, J. B., Senderek, J., and Suter, U. (2012) Myelin is dependent on the Charcot-Marie-Tooth Type 4H disease culprit protein FRABIN/FGD4 in Schwann cells. *Brain* **135,** 3567–3583
51. Cotter, L., Ozçelik, M., Jacob, C., Pereira, J. A., Locher, V., Baumann, R., Relvas, J. B., Suter, U., and Tricaud, N. (2010) Dlg1-PTEN interaction regulates myelin thickness to prevent damaging peripheral nerve overmyelination. *Science* **328,** 1415–1418
52. Goebbels, S., Oltrogge, J. H., Wolfer, S., Wieser, G. L., Nientiedt, T., Pieper, A., Ruhwedel, T., Groszer, M., Sereda, M. W., and Nave, K.-A. (2012) Genetic disruption of Pten in a novel mouse model of tomaculous neuropathy. *EMBO Mol. Med.* **4,** 486–499
53. Jung, Y.-S., Qian, Y., and Chen, X. (2010) Examination of the expanding pathways for the regulation of p21 expression and activity. *Cell. Signal.* **22,** 1003–1012
54. Borgdorff, V., Lleonart, M. E., Bishop, C. L., Fessart, D., Bergin, A. H., Overhoff, M. G., and Beach, D. H. (2010) Multiple microRNAs rescue from Ras-induced senescence by inhibiting p21(Waf1/Cip1). *Oncogene* **29,** 2262–2271
55. Takeuchi, S., Takahashi, A., Motoi, N., Yoshimoto, S., Tajima, T., Yamakoshi, K., Hirao, A., Yanagi, S., Fukami, K., Ishikawa, Y., Sone, S., Hara, E., and Ohtani, N. (2010) Intrinsic cooperation between p16INK4a and p21Waf1/Cip1 in the onset of cellular senescence and tumor suppression *in vivo*. *Cancer Res.* **70,** 9381–9390
56. Zhang, R., Poustovoitov, M. V., Ye, X., Santos, H. A., Chen, W., Daganzo, S. M., Erzberger, J. P., Serebriiskii, I. G., Canutescu, A. A., Dunbrack, R. L., Pehrson, J. R., Berger, J. M., Kaufman, P. D., and Adams, P. D. (2005) Formation of MacroH2A-containing senescence-associated heterochromatin foci and senescence driven by ASF1a and HIRA. *Dev. Cell* **8,** 19–30
57. Bouhy, D., and Timmerman, V. (2013) Animal models and therapeutic prospects for Charcot-Marie-Tooth disease. *Ann. Neurol.* **74,** 391–396
58. Young, P., and Sueter, U. (2005) in *Hereditary Peripheral Neuropathies* (Kuhlenbäumer, G., Stögbauer, F., Ringelstein, E. B., Young, P.) pp. 227–236, Steinkopff, Darmstadt
59. Parkinson, D. B., Bhaskaran, A., Arthur-Farraj, P., Noon, L. A., Woodhoo, A., Lloyd, A. C., Feltri, M. L., Wrabetz, L., Behrens, A., Mirsky, R., and Jessen, K. R. (2008) c-Jun is a negative regulator of myelination. *J. Cell Biol.* **181,** 625–637
60. Liu, J., Zhao, Y., Eilers, M., and Lin, A. (2009) Miz1 is a signal- and pathway-specific modulator or regulator (SMOR) that suppresses TNF-α-induced JNK1 activation. *Proc. Natl. Acad. Sci. U.S.A.* **106,** 18279–18284
61. Jessen, K. R., and Mirsky, R. (2008) Negative regulation of myelination: relevance for development, injury, and demyelinating disease. *Glia* **56,** 1552–1565
62. Huxley, C., Passage, E., Robertson, A. M., Youl, B., Huston, S., Manson, A., Sabéran-Djoniedi, D., Figarella-Branger, D., Pellissier, J. F., Thomas, P. K., and Fontés, M. (1998) Correlation between varying levels of PMP22 expression and the degree of demyelination and reduction in nerve conduction velocity in transgenic mice. *Hum. Mol. Genet.* **7,** 449–458
63. Sereda, M., Griffiths, I., Pühlhofer, A., Stewart, H., Rossner, M. J., Zimmerman, F., Magyar, J. P., Schneider, A., Hund, E., Meinck, H. M., Suter, U., and Nave, K. A. (1996) A transgenic rat model of Charcot-Marie-Tooth disease. *Neuron* **16,** 1049–1060
64. Gebhardt, A., Frye, M., Herold, S., Benitah, S. A., Braun, K., Samans, B., Watt, F. M., Elsässer, H.-P., and Eilers, M. (2006) Myc regulates keratinocyte adhesion and differentiation via complex formation with Miz1. *J. Cell Biol.* **172,** 139–149
65. van Riggelen, J., Müller, J., Otto, T., Beuger, V., Yetil, A., Choi, P. S., Kosan, C., Möröy, T., Felsher, D. W., and Eilers, M. (2010) The interaction between Myc and Miz1 is required to antagonize TGFβ-dependent autocrine signaling during lymphoma formation and maintenance. *Genes Dev.* **24,** 1281–1294
66. Seoane, J., Pouponnot, C., Staller, P., Schader, M., Eilers, M., and Massagué, J. (2001) TGFβ influences Myc, Miz-1 and Smad to control the CDK inhibitor p15INK4b. *Nat. Cell Biol.* **3,** 400–408
67. Romanov, V. S., Pospelov, V. A., and Pospelova, T. V. (2012) Cyclin-dependent kinase inhibitor p21(Waf1): contemporary view on its role in senescence and oncogenesis. *Biochemistry* **77,** 575–584